Journal of Fluids and Structures (2000) **14,** 819–851
doi:10.1006/jfls.2000.0302, available online at http://www.idealibrary.com on IDEAL®

NUMERICAL STUDY OF THE FLOW PAST A CYLINDER EXCITED TRANSVERSELY TO THE INCIDENT STREAM. PART 1: LOCK-IN ZONE, HYDRODYNAMIC FORCES AND WAKE GEOMETRY

P. Anagnostopoulos

Department of Civil Engineering, University of Thessaloniki Thessaloniki 54006, Greece

(Received 21 September 1998, and in final form 15 March 2000)

The numerical study of the flow past a circular cylinder forced to oscillate transversely to the incident stream is presented herein, at a fixed Reynolds number equal to 106. The finite element technique was favoured for the solution of the Navier–Stokes equations, in the formulation where the stream function and the vorticity are the field variables. The cylinder oscillation frequency ranged between 0·80 and 1·20 of the natural vortex-shedding frequency, and the oscillation amplitude extended up to 50% of the cylinder diameter. Since the resolution of the characteristics of synchronized wakes is the focus of the study, the first task is the determination of the boundary of the lock-in region. The computation revealed that, when the cylinder oscillation frequency exceeds the frequency of the natural shedding of vortices, the flow is not absolutely periodic at subsequent cycles but a quasiperiodic flow pattern occurs, which creates difficulty in the determination of the lock-in boundary. The time histories of the drag and lift forces for various oscillation parameters are presented, while the vorticity contours were favoured for the numerical flow visualization. The hydrodynamic forces, the phase angle between the lift force and the cylinder displacement, and the parameters of the wake geometry when steady state was reached, are presented in cumulative diagrams. These diagrams indicate the effect of the oscillation parameters on the hydrodynamic forces and on the wake geometry.

1. INTRODUCTION

It is well-known that at Reynolds numbers in excess of approximately 40 the wake of a circular cylinder in steady flow consists of two staggered rows of vortices, the vortices of each row being shed alternately from either side of the body. As the vortices are shed, a periodic force is exerted on the cylinder, whose component in the transverse direction (lift force) has the same frequency as the vortex-shedding cycle, while the frequency of its streamwise component (drag force) is equal to twice the shedding frequency. Vortex shedding can be dramatically changed when a cylinder oscillates in a flow stream, in the cross-flow or in the streamwise direction. In certain ranges of amplitude and frequency of oscillation the body motion can control the instability mechanism which leads to vortex shedding. One of the most interesting characteristics of this fluid–body interaction is that of synchronization, or "lock-in", between the vortex shedding and vibration frequencies. The vortex-shedding frequency diverges from that corresponding to a fixed cylinder and becomes equal to the frequency of the cylinder oscillation, when the oscillation amplitude exceeds a critical threshold.

These complicated flow–solid body interaction phenomena drew the attention of researchers in the last several decades. Bishop & Hassan (1964) investigated experimentally

0889–9746/00/080819 + 33 $35.00/0

the forced oscillations of a circular cylinder in the cross-flow direction, with special attention to the hydrodynamic forces exerted on the body, over a wide range of driving frequencies and oscillation amplitudes. Their experiments revealed the magnification of the mean drag and of the lift amplitude when the excitation frequency is close to the natural shedding frequency, and a sudden change in the phase angle between the lift force and cylinder displacement when the oscillation frequency is varied around the shedding frequency. Koopmann (1967) conducted a flow visualization study for the investigation of the effect of the cylinder excitation in the transverse direction on the vortex street wake. He found that synchronization of the vortex-shedding frequency with the cylinder oscillation frequency (lock-in) occurred above a threshold amplitude of oscillation, which became larger as the deviation of the oscillation frequency from the natural shedding frequency was increased. Moreover, he reported that the cylinder vibration resulted in the alignment of the vortex filaments with the cylinder axis, and the reduction of the lateral spacing of the vortices with increasing amplitude of oscillation. Honji & Taneda (1968) examined the vortex-street wake of a circular cylinder undergoing transverse oscillations in a uniform stream at Reynolds numbers between 70 and 163. They determined the extent of the lock-in region, and conducted flow visualization of the wake and measurements of the drag force. Griffin (1971) investigated the alterations of the geometry of the cylinder wake induced by different conditions of forced excitation from velocity measurements. His experiments revealed that the vortex formation length which was used as a characteristic parameter, is substantially influenced both by the frequency and the amplitude of the forced oscillations at lock-in. Griffin & Ramberg (1974) examined the effect of lateral cylinder vibrations on the geometry and vortex strength of a periodic wake. For the evaluation of the unknown parameters, the fluid velocities obtained from hot-wire measurements were matched with a mathematical model based on the Oseen vortex. Sarpkaya (1978) measured the hydrodynamic forces on a circular cylinder forced to oscillate transversely to the incident stream. He decomposed the total transverse force into in-phase and out-of-phase components which display abrupt jumps at resonance. Bearman & Currie (1979) measured the pressure on a circular cylinder oscillating transversely to the main flow at 90° from the leading edge, over a wide range of oscillation amplitudes and reduced velocities at lock-in. They found an abrupt phase jump between pressure at 90° and the cylinder displacement close to the resonant frequency. This result is in close agreement with Feng's (1968) measurements, in which an elastically mounted cylinder was free to oscillate transversely to the incident stream. Zdravkovich (1982) analysed the flow visualization patterns of previous investigators and suggested that the phase jump of the hydrodynamic forces can be explained by a change of the timing of the vortices being shed with respect to the displacement of the cylinder. Ongoren & Rockwell (1988) conducted a flow visualization study in the near wake of a sinusoidally excited circular cylinder using the hydrogen bubble technique. They noticed that when the cylinder oscillation frequency was lower than the natural shedding frequency, the vortices were shed when the cylinder had reached the amplitude on the same side. As the oscillation frequency was increased above the natural shedding frequency, the vortices were shed on the opposite side from which the amplitude of the cylinder displacement was reached. Williamson & Roshko (1988) conducted experiments at which the period of forced oscillation was varied up to three times the period of natural shedding and the amplitude up to five cylinder diameters. They observed a series of vortex-shedding patterns in the synchronization region, which they classified in terms of the number of vortices shed per oscillation cycle. One of the most interesting results of this research is that, if the reduced velocity exceeds a critical threshold for a given amplitude of oscillation, the vortex pattern diverges from that according to which two vortices are shed per oscillation cycle ("2S" mode) and takes the more complicated form at which two pairs of

vortices are shed per oscillation cycle ("2P" mode). The same investigators attributed the phase jump near resonance established from the force measurements of Bishop & Hassan (1964) to the sudden transition between these two modes, since this very important study was based on flow visualization and did not comprise force measurements. Gopalkrishnan (1993) measured the hydrodynamic forces on a transversely excited cylinder in a water channel, undergoing sinusoidal and beating oscillations. Brika & Laneville (1993) examined the cross-flow oscillations of a long flexible cylinder and obtained hysteresis loops in the oscillation amplitudes. They observed that, for the same stream velocity, the high-amplitude branch is associated with the 2P mode, while the low-amplitude branch of the loop with the 2S mode. More recently, Gu *et al.* (1994) conducted a flow visualization study at Reynolds numbers 185 and 5000 using PIV and PTV techniques. They confirmed the effect of the cylinder oscillation frequency on the timing of vortex shedding observed in previous investigations and, most importantly, they noticed the existence of two saddle points in the streamline pattern, when the cylinder oscillation frequency exceeds the natural shedding frequency.

Apart from the experimental studies, numerical solutions of flow around oscillating cylinders have been conducted in the last three decades, favoured by the enormous increase in power of digital computers. Sarpkaya & Shoaff (1979) employed a discrete vortex method for the solution of vortex-excited oscillations of a circular cylinder at similar conditions with those of the experimental investigation conducted by Feng (1968) at subcritical Reynolds numbers. Hurlbut *et al.* (1982) favoured finite-difference methods for the solution of flow about a cylinder oscillating in the streamwise and in the transverse direction. Chilukuri (1987) used a finite difference scheme for the solution of flow past transversely vibrating cylinders, while Lecointe & Piquet (1989) investigated numerically the vortex-shedding characteristics behind a circular cylinder performing in-line and lateral oscillations. Mittal & Tezduyar (1992) simulated numerically the transverse oscillations of an elastically mounted cylinder at Reynolds numbers extending up to 360 using the finite element technique. Nomura (1993), Anagnostopoulos (1994) and Wei *et al.* (1995) investigated the flow past an elastically mounted cylinder in the stable range ($Re < 150$) employing finite element schemes, and used the experimental results by Anagnostopoulos & Bearman (1992) for the validation of their results. Meneghini & Bearman (1995) used a discrete vortex method for the simulation of oscillatory flow past a circular cylinder at $Re = 200$. They performed computations in which the frequency of the oscillatory flow was varied around the natural shedding frequency while the oscillation amplitude was extending up to 60% of the cylinder diameter, and they determined the boundary of the lock-in region. On the other hand, Copeland & Cheng (1995) focussed their attention on low oscillation amplitudes at $Re = 200$, using a spectral element technique. They noticed that when the cylinder was forced to oscillate at a frequency higher than that of the natural vortex shedding, the hydrodynamic forces displayed an aperiodic character, accompanied by alterations in the flow pattern. Lu & Dalton (1996) conducted a numerical study of flow around a cylinder excited transversely at Reynolds numbers equal to 185, 500 and 1000, for various oscillation frequencies and amplitudes. Their numerical visualization results revealed that the oscillation frequency at which vortex switching occurs decreases slightly with increasing Reynolds number. The flow pattern they obtained at $Re = 185$ agrees favourably with that derived experimentally by Gu *et al.* (1994). Akbari & Price (1997) employed a vortex method for the simulation of the flow around a transversely oscillating cylinder at Reynolds numbers ranging between 200 and 1000. They found that when the cylinder oscillation frequency exceeded the natural shedding frequency, lock-in occurred at higher amplitudes than those observed experimentally by Koopmann (1967) and numerically by Meneghini & Bearman (1995). Another study is that by Zhang & Dalton (1997), who simulated numerically the

forced oscillation of a cylinder in the cross-flow direction at Reynolds numbers equal to 200 and 850, employing a finite difference technique.

In the present study, the numerical solution of flow past a cylinder forced to oscillate transversely to the incident stream was conducted, using the finite element technique. The Reynolds number was held constant equal to 106, equal to that of a related study concerning the flow around a fixed cylinder (Anagnostopoulos 1997). The first task of the study was the determination of the boundary of the lock-in region. Afterwards, computations at various conditions of the cylinder excitation were conducted, in which, f_r, which denotes the ratio of the cylinder oscillation frequency, f_c, to the natural shedding frequency, f_s, was varied between 0·80 and 1·20, and the oscillation amplitude, A, was increased to 50% of the cylinder diameter. The time histories of the hydrodynamic forces in nondimensional form are presented, while the equivorticity lines were favoured for the determination of the wake geometry. To elucidate the effect of the transverse cylinder motion on the hydrodynamic forces and on the cylinder wake, the mean drag, the lift amplitude, the phase angle between the lift force and the cylinder displacement, and the parameters of the wake geometry when steady state was reached are illustrated in cumulative diagrams. Although the study was conducted at a low Reynolds number in order to facilitate the solution and make comparisons with available experimental data, more general conclusions can be extracted, which are applicable to flows at higher Reynolds numbers.

2. THE COMPUTATIONAL TECHNIQUE

2.1. The Governing Equations

The method used in the present study is similar to that employed by Anagnostopoulos (1989, 1994) for the simulation of flow around a vortex-excited cylinder in the transverse direction. The mathematical model of the problem consists of the Navier–Stokes equations, in the formulation where the stream function, Ψ, and the vorticity, ζ, are the field variables. If n and $n+1$ are two successive time levels separated by a time Δt, the governing equations become

$$\nabla^2 \Psi_n = -\zeta_n, \tag{1}$$

$$\frac{\partial \zeta_n}{\partial t} + \frac{\partial \Psi_n}{\partial y}\frac{\partial \zeta_n}{\partial x} - \frac{\partial \Psi_n}{\partial x}\frac{\partial \zeta_n}{\partial y} = \nu \nabla^2 \zeta_{n+1}. \tag{2}$$

2.2. The Boundary Conditions and the Computational Mesh

The finite element mesh used by Anagnostopoulos (1997) for the numerical visualization of the flow pattern around a fixed cylinder, was also employed in the present solution. It contains 5801 nodes and 11 244 three-node triangular elements.

On the inflow boundary, the boundary condition for the stream function is $\partial \Psi / \partial y = U$, where U is the free-stream velocity. The stream function was considered constant along the boundaries parallel to the approaching stream, while the vorticity was taken equal to zero on the inflow boundary and along the external boundaries parallel to the incident stream. These boundary conditions represent the flow in a channel without friction on the channel walls. On the outflow boundary the boundary conditions for the stream function and the vorticity were approximated by setting their derivatives in the direction normal to the boundary equal to zero.

The boundary condition for the stream function on the cylinder surface is derived from the impermeability condition, namely

$$\frac{\partial \Psi}{\partial s} = - U_c \sin\theta, \tag{3}$$

where U_c is the instantaneous cylinder velocity, and s the tangential direction shown together with its perpendicular n in Figure 1.

The vorticity on the cylinder boundary is given by

$$\zeta = \frac{\partial v}{\partial s} - \frac{\partial^2 \Psi}{\partial n^2}. \tag{4}$$

The impermeability condition yields

$$\frac{\partial v}{\partial s} = \frac{U_c}{r}\cos\theta; \tag{5}$$

therefore, equation (4) becomes

$$\zeta = \frac{U_c}{r}\cos\theta - \frac{\partial^2 \Psi}{\partial n^2}. \tag{6}$$

Assuming linear interpolation of the vorticity between the nodal points A and B of Figure 1 and integrating over the length Δn of the segment AB we obtain

$$\int_0^{\Delta n} \left(\frac{U_c}{r}\cos\theta - \frac{\partial^2 \Psi}{\partial n^2}\right) \mathrm{d}n = \int_0^{\Delta n} \left[\left(1 - \frac{n}{\Delta n}\right)\zeta_A + \frac{n}{\Delta n}\zeta_B\right] \mathrm{d}n. \tag{7}$$

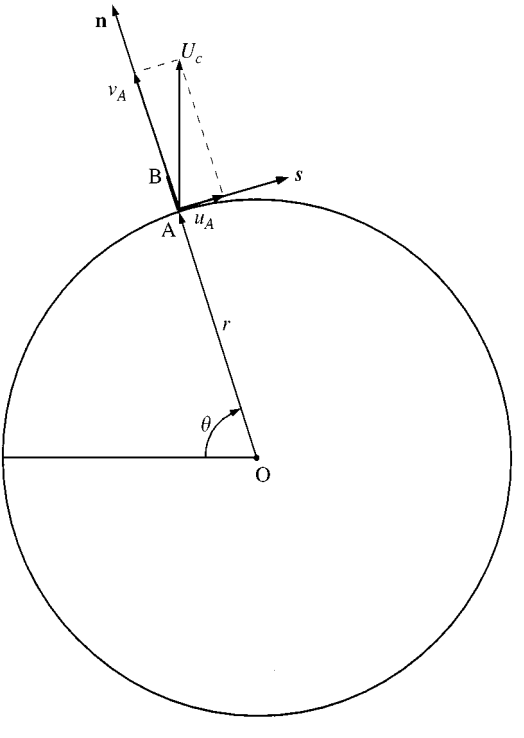

Figure 1. Definition sketch.

The integration of equation (7) yields

$$\zeta_A = \frac{3}{\Delta n^2}(\Psi_A - \Psi_B) - \frac{\zeta_B}{2} + 1{\cdot}5\frac{U_c}{r}\cos\theta, \tag{8}$$

which is the expression used for the evaluation of the vorticity on the cylinder in the present study. Equation (8), although somewhat different from those used previously by Anagnostopoulos (1989, 1994) for the evaluation of the vorticity generated on a transversely oscillating cylinder, was favoured in the present investigation for reasons of consistency with the related study for a fixed cylinder (Anagnostopoulos 1997).

2.3. The Finite Element Equations and the Solution Algorithm

Applying Galerkin's method to equations (1) and (2) for each element and assembling for the whole domain, the following equations are obtained:

$$[K_1]\{\Psi\}_n = [K_2]\{\zeta\}_n + \{R_1\}, \tag{9}$$

$$[K_3]\{\zeta\}_{n+1} = [K_4]\{\zeta\}_n - \{R_2\} + \{R_3\}, \tag{10}$$

where $[K_1]$, $[K_2]$, $[K_3]$ and $[K_4]$ are square matrices, whereas $\{R_1\}$, $\{R_2\}$ and $\{R_3\}$ are column vectors.

Since the position of the oscillating cylinder changes at different time levels, the computational grid was translated with the cylinder, and the nodal values of vorticity calculated from equation (10) were interpolated linearly to new grid locations, as described by Anagnostopoulos (1989).

Thus, the solution algorithm consists of the following steps:

(a) evaluation of the stream function at the time level n from equation (9); the values of vorticity calculated in the previous iteration have been interpolated to the grid locations of the present time level, except from those lying on the solid boundary;
(b) the vorticity values at the no-slip boundary are derived from equation (8);
(c) the nodal values of vorticity at the time level $n + 1$ are calculated from equation (10).

2.4. Calculations of Pressure, Shear and Hydrodynamic Forces

The pressure distribution throughout the flow field can be derived from Poisson's equation

$$\frac{\partial^2 p}{\partial x^2} + \frac{\partial^2 p}{\partial y^2} = -2\rho\left(\frac{\partial u}{\partial y}\frac{\partial v}{\partial x} - \frac{\partial u}{\partial x}\frac{\partial v}{\partial y}\right), \tag{11}$$

where ρ is the fluid density and u and v are the two components of the fluid velocity, evaluated from the values of the stream function. The equation of motion along the radial direction on the cylinder surface yields the boundary condition for pressure on the cylinder as

$$\frac{\partial p}{\partial n} = \mu\frac{\partial \zeta}{\partial s} + \rho A_c \cos\theta, \tag{12}$$

where μ is the viscosity of the fluid and A_c is the instantaneous cylinder acceleration.

The application of Galerkin's method to equation (11) for an element e and assembly throughout the domain yields

$$[K_5]\{p\} = \{R_4\} + \{R_5\} \tag{13}$$

in which $[K_5]$ is a square matrix, while $\{R_4\}$ and $\{R_5\}$ are column vectors. The element r_{5i} of the column vector $\{R_5\}$ is given from

$$r_{5i} = \int_S \frac{\partial p}{\partial n}\,\mathrm{d}s. \tag{14}$$

The integration is performed only on the cylinder surface, where a natural boundary condition for pressure is specified, according to equation (12).

The shear stress on the cylinder can be calculated from

$$\tau_w = \frac{2\mu}{r} U_c \cos\theta - \mu\zeta_w, \tag{15}$$

where ζ_w denotes the vorticity on the cylinder.

The drag and lift forces per unit cylinder length are calculated from the integration of shear stress and pressure around the cylinder:

$$F_D = \int_0^{2\pi} p\cos\theta\,\mathrm{d}\theta + \int_0^{2\pi} \tau_w \sin\theta\,\mathrm{d}\theta, \tag{16}$$

$$F_L = -\int_0^{2\pi} p\sin\theta\,\mathrm{d}\theta + \int_0^{2\pi} \tau_w \cos\theta\,\mathrm{d}\theta, \tag{17}$$

where θ is the angle defining the location of the point considered from the leading edge of the cylinder in the clockwise direction, as shown in Figure 1. From F_D and F_L, the nondimensional coefficients C_D and C_L can be derived, according to

$$C_D = \frac{F_D}{\frac{1}{2}\rho U^2 D} \quad \text{and} \quad C_L = \frac{F_L}{\frac{1}{2}\rho U^2 D}, \tag{18}$$

where D denotes the cylinder diameter.

3. APPLICATION AND RESULTS

The numerical simulations in the present investigation were conducted at Re = 106. The Reynolds number was kept equal to that used for the numerical study of flow past a fixed cylinder (Anagnostopoulos 1997), in order to compare the results when the cylinder oscillates at various frequencies and amplitudes with those of the fixed cylinder case. As stated earlier, the cylinder oscillation frequency, f_c, was varied between 0·80 and 1·20 of the Strouhal frequency, f_s, and the oscillation amplitude, A, was extended to 50% of a cylinder diameter.

In all cases the cylinder was excited sinusoidally, and its motion started from the position of minimum displacement. The corresponding equation of motion is

$$y = A\sin(\omega_c t - \pi/2), \tag{19}$$

where ω_c is the circular frequency of oscillation, equal to $2\pi f_c$. The starting solution for the flow field was the fully developed vortex street around a fixed cylinder, as derived by Anagnostopoulos (1997). The solution continued until the flow pattern and the hydrodynamic forces became periodic or quasiperiodic. Quasiperiodic motion occurs outside lock-in, or when the cylinder oscillation frequency is higher than the natural shedding frequency, as will be explained later. In many cases periodicity or quasiperiodicity was reached after many oscillation cycles from the inception of the cylinder oscillation, thus extensive computer resources were required.

For each case considered, the solution yielded the distribution of stream function, vorticity and pressure throughout the solution domain, while the hydrodynamic forces on the cylinder were evaluated from equations (16) and (17). As in the related study for a fixed cylinder, the equivorticity lines generated from the vorticity distribution were favoured for the determination of the wake geometry, since the points where the absolute value of vorticity becomes maximum mark clearly the centres of the vortices.

3.1. The Lock-in Region

One of the most interesting characteristics of the fluid–body interaction is that of synchronization, or "lock-in", between the vortex shedding and the cylinder vibration frequencies. When the wake is synchronized, the vortex-shedding frequency diverges from that corresponding to a fixed cylinder and becomes equal to the frequency of the cylinder oscillation. Experiments for the determination of the lock-in region of a cylinder forced to oscillate transversely to the incident stream have been conducted by Koopmann (1967), Stansby (1976) and Cheng & Moretti (1991), and computations by Lecointe & Piquet (1989), Meneghini & Bearman (1995) and Akbari & Price (1997). The lock-in region boundaries derived from the experiments by Koopmann (1967) and Stansby (1976) have been superimposed by Blevins (1994). The fitting curves drawn by Blevins (1994; p. 55, figure 3–10) in order to define the lock-in boundaries for the various frequency ratios examined, are shown to be symmetrical with respect to the vertical line through $f_r = 1$. Although for $f_r < 1$ the limit of the lock-in zone derived from the numerical studies by Meneghini & Bearman and Akbari & Price, quoted previously, displays considerable agreement with experiment, synchronization is observed at an amplitude higher than the experimental when f_r exceeds unity.

It should be noted that, in the experiments the lock-in boundary was determined from fluid velocity traces, whereas in the computational studies from the hydrodynamic forces. Experimental velocity records used for the determination of the lock-in zone of a cylinder oscillating transversely at $A/D = 0{\cdot}20$, have been presented by Honji & Taneda (1968). Although the measurement of the hydrodynamic forces, especially at low Reynolds numbers, is a rather difficult task, their derivation from a computational solution is straightforward. Since within the lock-in region the vortex-shedding frequency is coincident with the frequency of the cylinder oscillation, it was thought that the periodicity of the hydrodynamic forces, especially of that in the transverse direction at a prominent frequency equal to the cylinder oscillation frequency, constitutes a simple and safe criterion for the determination of synchronization. Bearing the quoted discrepancy between computation and experiment when f_r exceeds 1 in mind, the determination of the boundaries of the lock-in region was the first task of the present numerical study.

Computational tests were conducted for all frequency ratios considered in the present study, except for the case when $f_r = 1$. For each frequency ratio, the computation started with a low oscillation amplitude, which was increased in $0{\cdot}01D$ steps, until the wake became synchronized. The solution revealed differences in the flow when f_r was exceeding 1 from the cases in which $f_r < 1$, therefore these two cases are examined separately.

In the range of frequency ratios lower than 1, when the flow was unlocked, the traces of the hydrodynamic forces were not periodic but appeared in modulated form. The time records of the fluid velocities in the streamwise direction after an initial transient exhibited also beating behaviour. As an example, the traces of the hydrodynamic forces for $f_r = 0{\cdot}90$ and $A/D = 0{\cdot}08$ just outside lock-in are presented in Figure 2(a), from the 10th period onwards. In all force traces presented in this study, the time base is the real time t divided by the cylinder oscillation period, denoted as T_c. According to equation (19), the cylinder reaches its lowermost position at the beginning of each oscillation cycle. After a transient

state of approximately 16 periods from the inception of the cylinder oscillation in which the mean drag and the lift amplitude are magnified, the hydrodynamic forces become modulated. The power spectrum of the lift force depicted in Figure 2(b), displays a peak at a frequency slightly lower than the natural shedding frequency. The traces of the fluid velocity were also modulated, and the vortex-shedding frequency determined from these traces was found to be infinitesimally (by 0·8%) higher than the cylinder oscillation frequency at these excitation conditions close to the lock-in boundary. Therefore, when the cylinder oscillates at $f_r = 0{\cdot}90$ and $A/D = 0{\cdot}08$, although the flow remains unlocked, it is affected strongly by the cylinder motion, displaying different characteristics from the fixed cylinder case. This is a typical example of the "receptivity zone", as defined by Karniadakis & Triantafyllou (1989).

When the frequency ratio exceeds unity, the situation becomes more complicated. Numerical tests at this range revealed that the hydrodynamic forces were not periodic at subsequent cycles but exhibited beats for all oscillation amplitudes examined, except for the value $A/D = 0{\cdot}50$. In spite of the modulation, the average frequency of the lift force is equal to the cylinder oscillation frequency, as illustrated for the sample case $f_r = 1{\cdot}10$ and $A/D = 0{\cdot}10$, depicted in Figure 3(a). The power spectrum of the lift force displayed in Figure 3(b) shows clearly that the prominent frequency is equal to the cylinder oscillation frequency, whereas a smaller component can be seen at a frequency approximately 85% of f_c. When the oscillation amplitude was increased, the intensity of beating was reduced, as will be shown later.

In an attempt to clarify the situation, the time history of the streamwise fluid velocity was also examined. Since, by definition, lock-in is the situation where the vortex-shedding frequency coincides with the cylinder oscillation frequency, it was thought instructive to determine the vortex-shedding frequency from velocity traces and compare it with the cylinder oscillation frequency. As an example, the time history of the streamwise component of the fluid velocity for $f_r = 1{\cdot}10$ and A/D equal to 0·10, 0·12, 0·13 and 0·20 is displayed in Figure 4(a–d). The velocity traces of Figure 4 correspond to a point located at a distance $x/D = 1{\cdot}28$ and $y/D = -0{\cdot}64$ from the centre of the cylinder cross-section. In all these figures, low-frequency periodicity is detectable, apart from the frequency corresponding to the shedding of vortices at successive cycles. In spite of the fluctuations of the velocity signal observed between different cycles, the time required for the shedding of a number of consecutive vortices is equal, or very close, to the time required for the completion of the same number of cylinder oscillation cycles. This becomes evident comparing the period of the low-frequency beats to the cylinder oscillation period. In Figure 4(b), for example, after the initial transient in the first 10 cycles, a sequence of beats is observed, the period of which is alternatively five and seven oscillation cycles. On the other hand, in Figure 4(d), the period of each low-frequency beat is equal to four oscillation cycles.

The power spectra in Figure 5(a–d) generated from the velocity traces of Figure 4(a–d) are illuminating. In Figure 5(a) which corresponds to $A/D = 0{\cdot}10$, three peaks are detectable; one at a frequency by 1·5% lower than the cylinder oscillation frequency, another equal to 85% of the oscillation frequency, while the prominent peak corresponds to 18% of f_c and is associated with the low-frequency modulation. The peak at 85% of f_c is in accord with that observed at the same frequency in the power spectrum of the lift force, depicted in Figure 3(b). As the oscillation amplitude is increased to 12% of the diameter, a peak exists in Figure 5(b) at a frequency by 0·8% lower than the cylinder oscillation frequency, while another is detectable at the natural shedding frequency. The peaks at 85% of f_c and those corresponding to the low-frequency modulation are still present. When the oscillation amplitude is increased to 13% of a diameter, the prominent frequency is absolutely coincident with the cylinder oscillation frequency, while the components at 82% of f_c and of

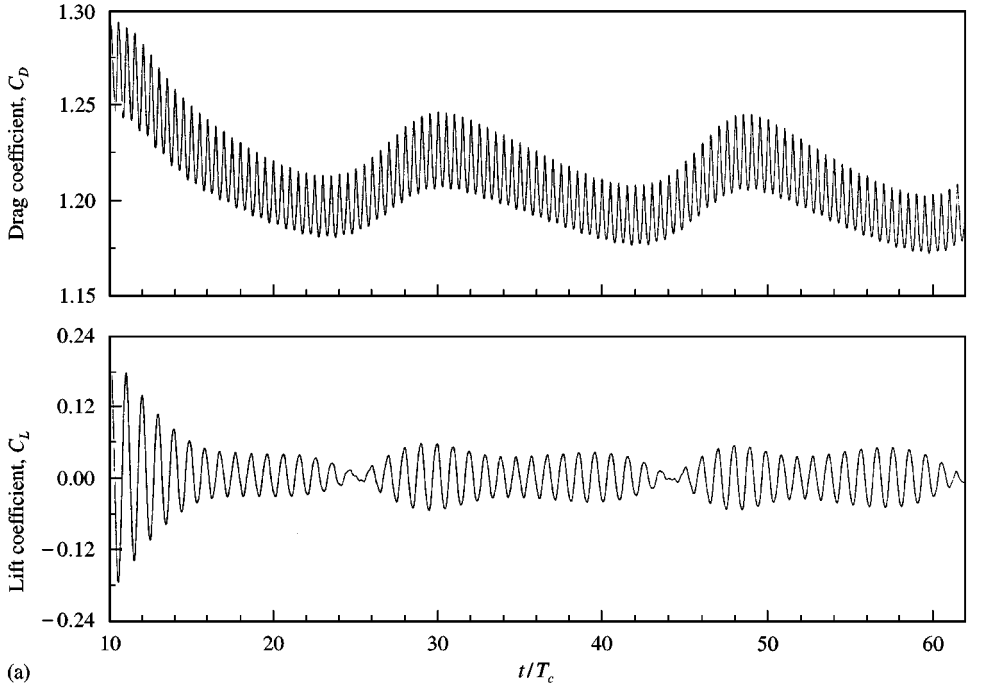

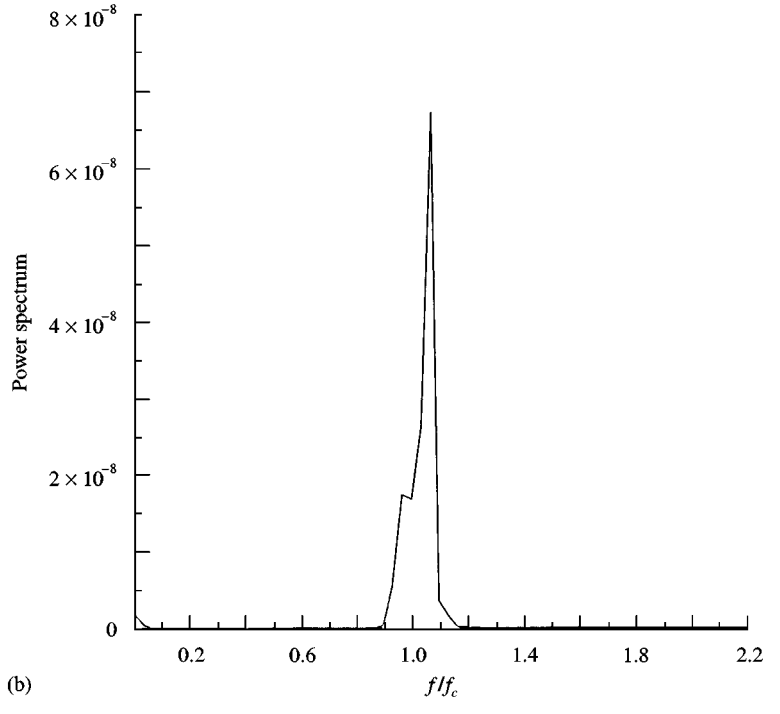

Figure 2. (a) Time history of the hydrodynamic forces, expressed as force coefficients, for $f_r = 0{\cdot}90$ and $A/D = 0{\cdot}08$ (outside lock-in); (b) the corresponding power spectrum of the lift force trace.

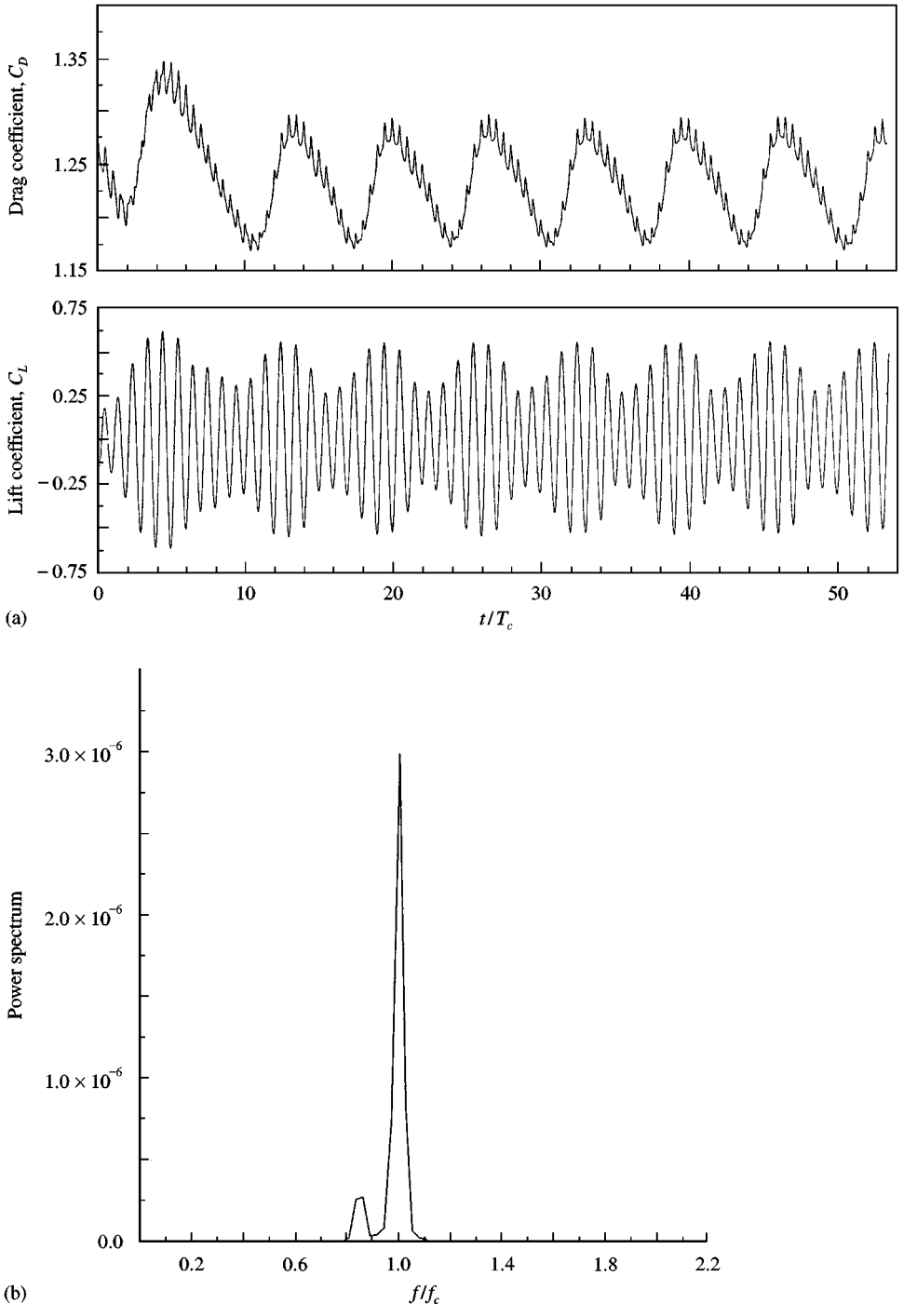

Figure 3. (a) Time history of the hydrodynamic forces for $f_r = 1{\cdot}10$ and $A/D = 0{\cdot}10$ (outside lock-in); (b) the corresponding power spectrum of the lift force trace.

the low-frequency beats are also detectable, although at a lower level. When the amplitude becomes 20% of a diameter, the prominent component at the cylinder oscillation frequency and another peak at 77% of f_c are present, as depicted in Figure 5(d).

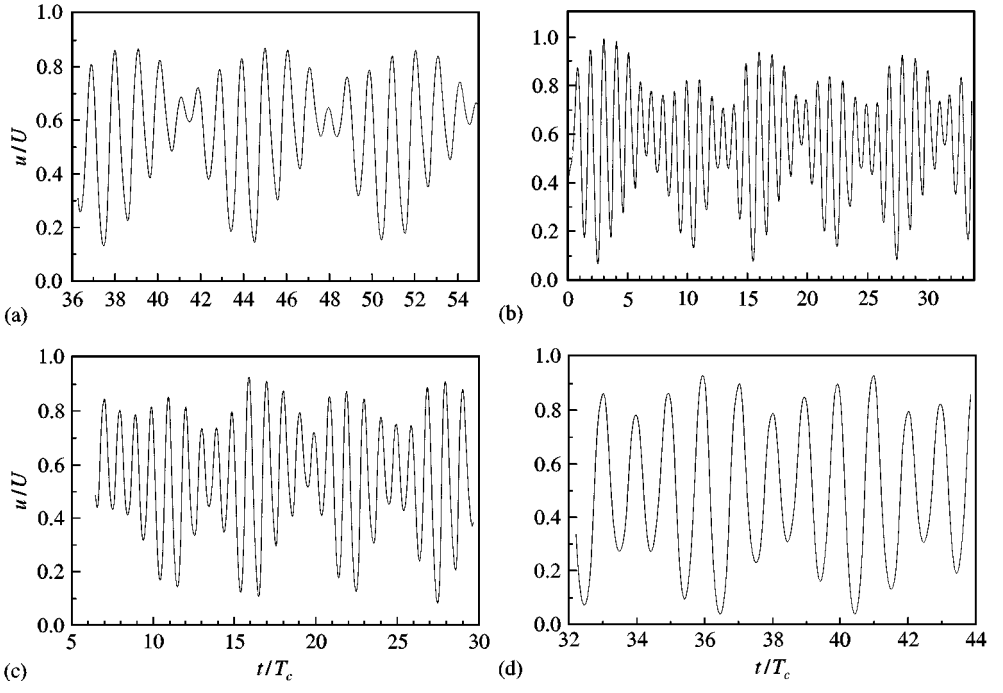

Figure 4. Traces of the streamwise velocity for various oscillation amplitudes at $f_r = 1{\cdot}10$: (a) $A/D = 0{\cdot}10$; (b) $A/D = 0{\cdot}12$; (c) $A/D = 0{\cdot}13$; (d) $A/D = 0{\cdot}20$. The coordinates of the point of measurement are $x/D = 1{\cdot}28$ and $y/D = -0{\cdot}63$ from the cylinder centre.

The power spectra of Figure 5(a–d) reveal the existence of peaks at frequencies ranging between 77 and 85% of the cylinder oscillation frequency. These peaks can be interpreted with reference to the velocity traces of Figure 4(a–d). In some cases the fluctuation of the velocity trace which corresponds to a specific vortex-shedding cycle is much less intense, which has a result the apparent reduction of the number of vortices shed during one beating period by one. For example, in Figure 4(a), when t/T_c equals 41 or 48, the fluctuation of the velocity signal is small. Although seven shedding cycles are clearly detectable in the first low-frequency beat and six in the second, the small velocity fluctuations quoted previously may give the impression of the shedding of six vortices during the first beat and five vortices during the second. The situation is more pronounced in velocity traces at the same streamwise distance from the cylinder, but closer to the wake centreline. Conversely, in velocity records at a large lateral distance from the wake centreline, cycle-to-cycle fluctuations were suppressed. This "competition" of the vortex-shedding frequency resulting from the velocity traces is responsible for the prominent peak at 85% of the cylinder oscillation frequency in Figure 5(a), apart from that very close to f_c. The same reasoning can be used for all other cases of Figure 5. In Figure 4(d), for example, the weakest velocity fluctuation in a four-period beat contributes to a frequency component equal to $0{\cdot}75f_c$, which is in close agreement with the peak at 77% of f_c displayed in the corresponding power spectrum of Figure 5(d).

Consequently, if the power spectrum contains a prominent frequency absolutely equal to the cylinder oscillation frequency as in Figure 5(c, d), the wake can be considered as "locked", although other frequencies may be present at a lower level. Therefore, for the determination of the lock-in boundary when $f_r > 1$, the power spectra were generated from the fluid velocity traces. When the prominent frequency was absolutely equal to the cylinder

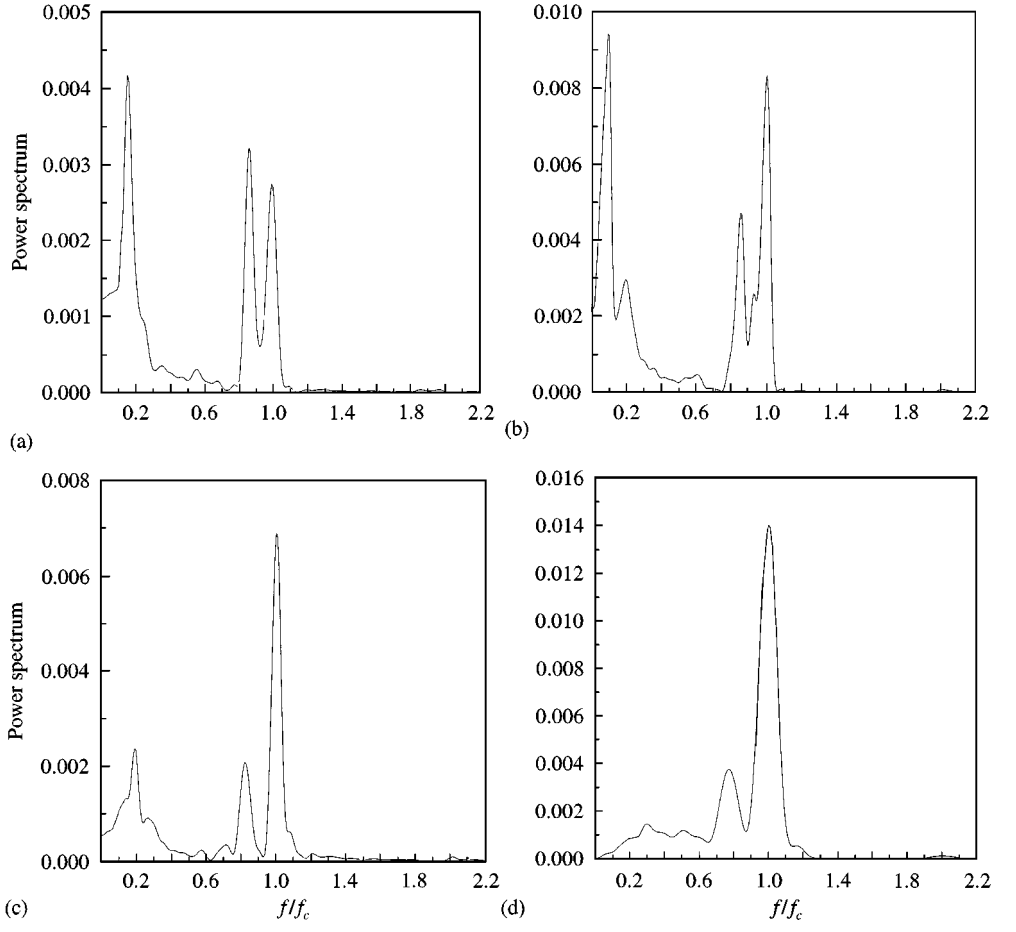

Figure 5. Power spectra of the streamwise velocity traces depicted in Figure 4: (a) $A/D = 0{\cdot}10$; (b) $A/D = 0{\cdot}12$; (c) $A/D = 0{\cdot}13$; (d) $A/D = 0{\cdot}20$.

oscillation frequency, as in the case illustrated in Figure 5(c) where $f_r = 1{\cdot}10$ and $A/D = 0{\cdot}13$, the wake was characterized as "synchronized". It is evident that, for a constant frequency ratio, synchronization persisted for a further increase of the amplitude. It should also be stressed that in some cases the receptivity zone may be very extended. For $f_r = 1{\cdot}20$ for example, although an absolutely synchronized wake is observed at $A/D = 0{\cdot}20$, the vortex-shedding frequency is just by 0·7% lower than the cylinder oscillation frequency, at an amplitude equal to 12% of a diameter.

The boundaries of the lock-in region are shown in Figure 6. For $f_r < 1$ they are similar to those found experimentally by Koopmann (1967) at Re = 100, whereas for $f_r > 1$ lock-in occurs at higher oscillation amplitudes than in the experiment, except from the case $f_r = 1{\cdot}20$. It should be stressed that the results of experimental studies at higher Reynolds numbers (Stansby 1976; Cheng & Moretti 1991) are qualitatively similar to Koopmann's, indifferently if f_r is greater or lower than 1.

From the previous discussion it has become evident that, when the oscillation amplitude exceeded a threshold, although the velocity traces were not periodic at consecutive cycles, the time required for the shedding of a number of successive vortices, was absolutely equal to the time required for the completion of the same number of oscillation cycles. It seems,

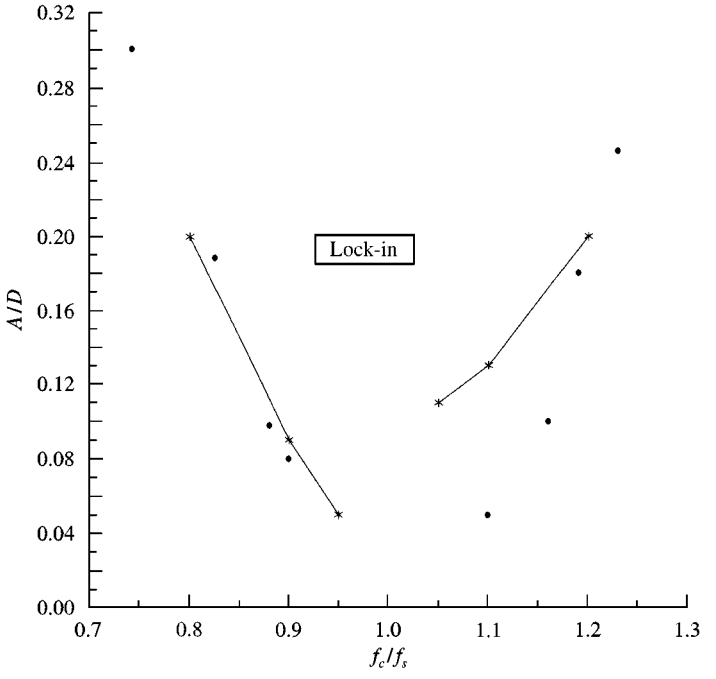

Figure 6. Boundary of the lock-in region: ✳, present study; •, experiments by Koopmann (1968).

therefore, that for $f_r > 1$ there exists a mechanism which renders the wake aperiodic, although the wake can be considered as locked. The aperiodic character of the wake reflects on the time history of the hydrodynamic forces. Thus, for $f_r > 1$ the periodicity of force traces seems to constitute a misleading criterion for the assessment of synchronized conditions; therefore, the velocity traces should be used for the determination of the lock-in zone.

The lack of agreement between computations and experiments at $f_r > 1$ has intrigued Griffin & Hall (1995), who attributed the fact to differences in fluid media and limitations imposed by the two-dimensional computations. Although the two-dimensional character of the computations may constitute a serious restriction, the previous reasoning provides a good explanation for the discrepancy, if the cycle-to-cycle periodicity of the hydrodynamic forces is used as the criterion of a synchronized wake. The discrepancy with the experiment, which still exists at $f_r > 1$ when the velocity traces are used for the determination of vortex-shedding frequency from a power spectrum, may be attributed to an uncertainty, owing to the great extent of the receptivity zone.

3.2. The Hydrodynamic Forces

The time histories of the nondimensional drag and lift forces on the cylinder for various amplitudes and frequencies of oscillation within the lock-in region are depicted in Figures 7–18. When $f_r \leq 1$, the hydrodynamic forces undergo a transient in the initial periods of the cylinder motion and then become fully periodic. For a constant frequency ratio, the establishment of periodicity is faster as the oscillation amplitude is increased. A component at the first harmonic is detectable in the traces of the drag force, which becomes less pronounced as the oscillation amplitude increases. Moreover, Figures 9–11 dictate that, when f_r diverges from 1, the time history of the lift force is not absolutely

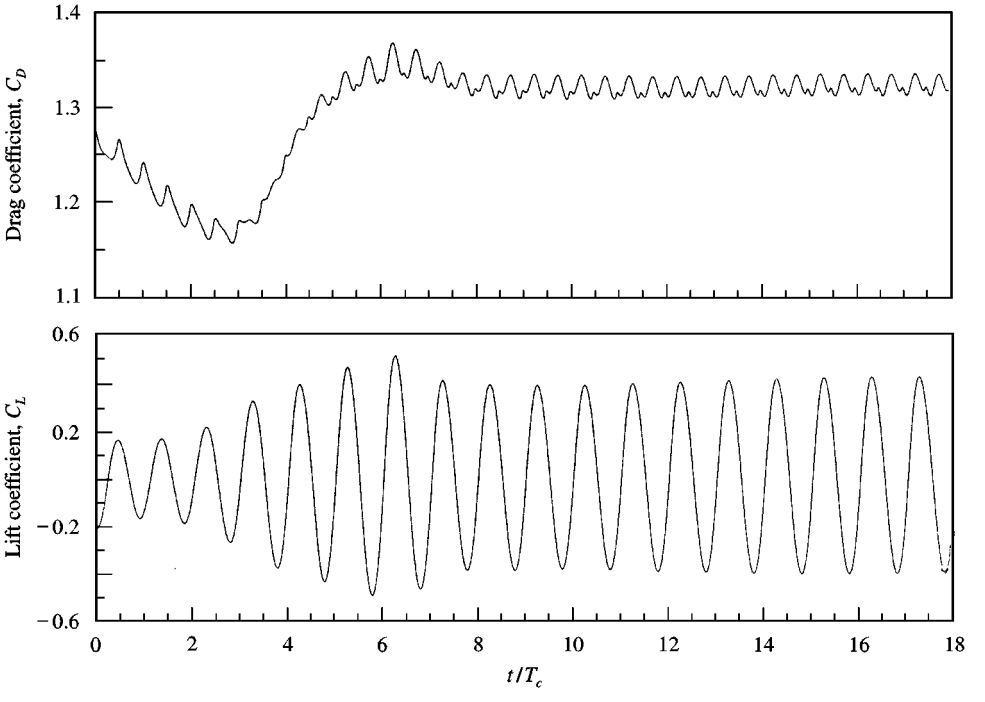

Figure 7. Time history of the hydrodynamic forces for $f_r = 1$ and $A/D = 0{\cdot}10$.

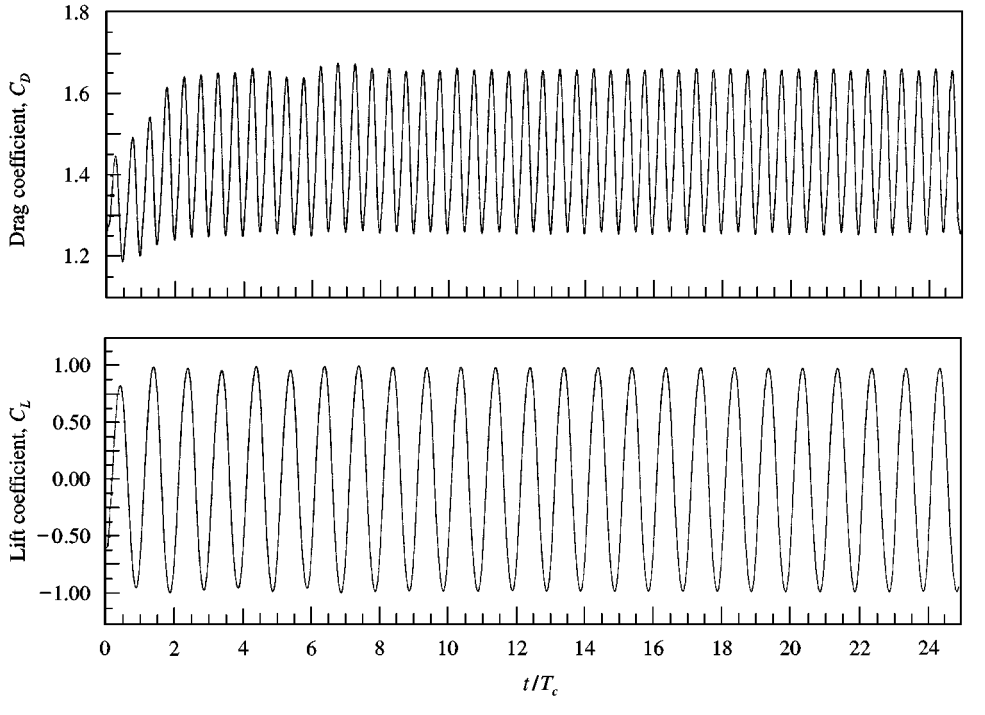

Figure 8. Time history of the hydrodynamic forces for $f_r = 1$ and $A/D = 0{\cdot}40$.

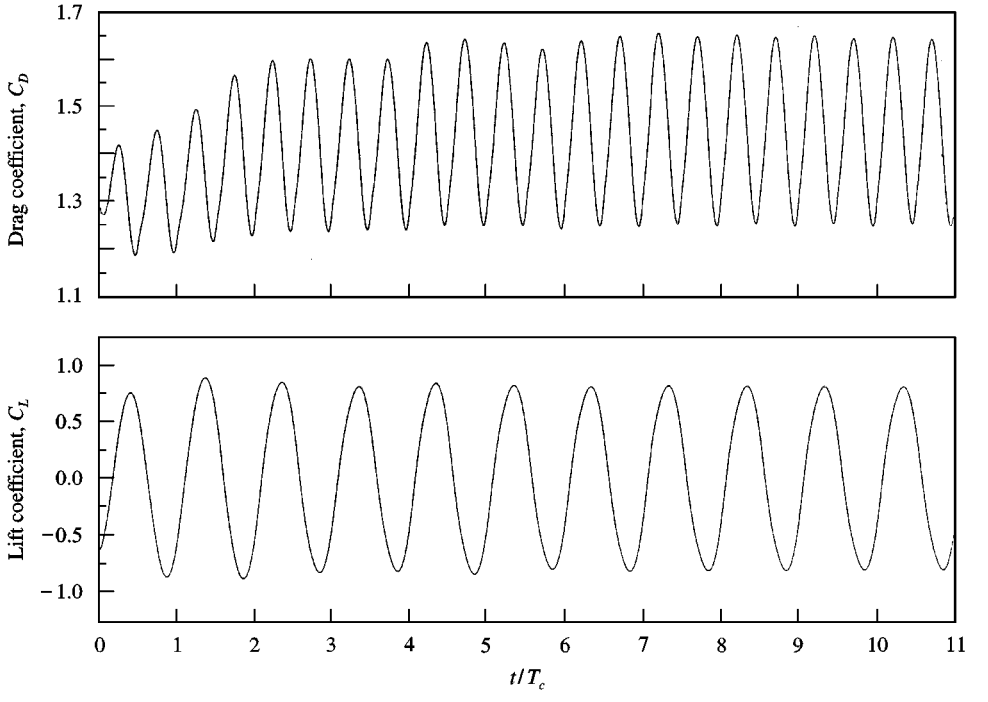

Figure 9. Time history of the hydrodynamic forces for $f_r = 0{\cdot}95$ and $A/D = 0{\cdot}40$.

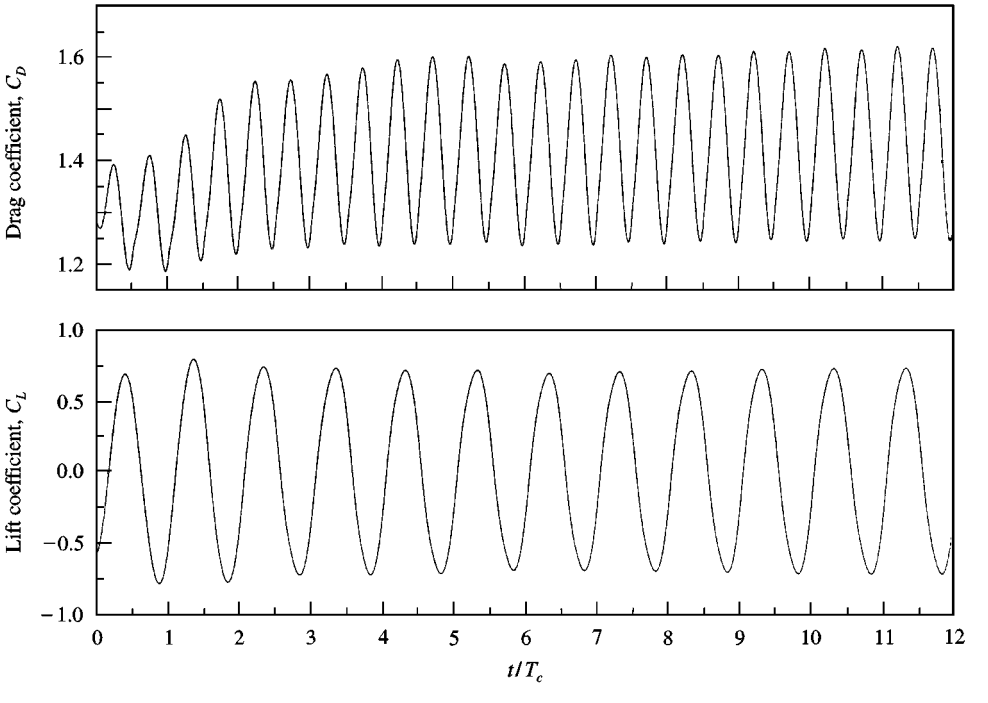

Figure 10. Time history of the hydrodynamic forces for $f_r = 0{\cdot}90$ and $A/D = 0{\cdot}40$.

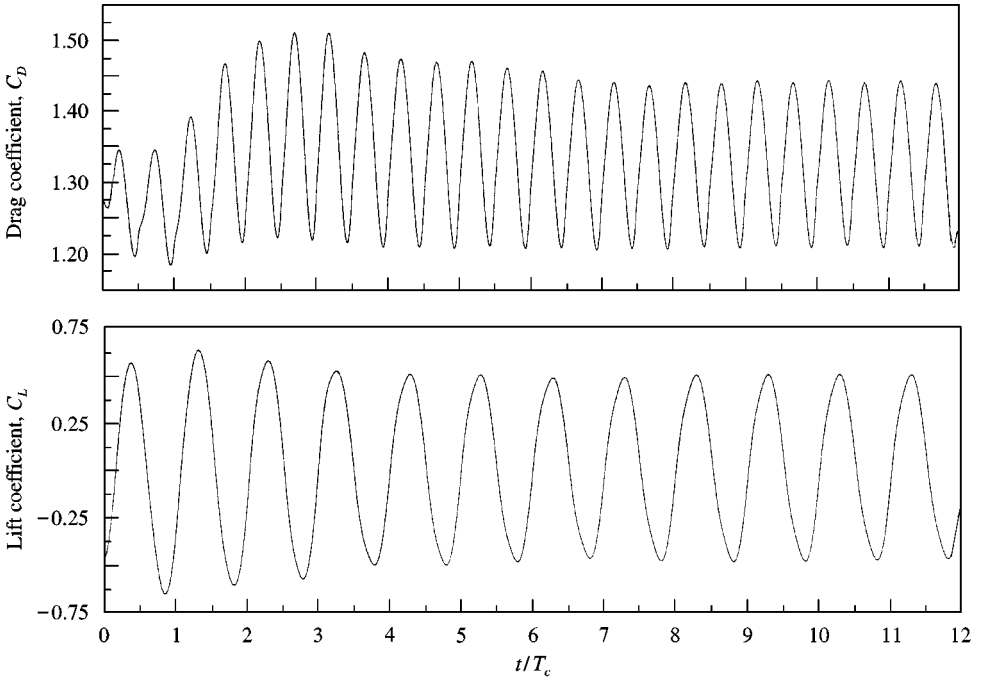

Figure 11. Time history of the hydrodynamic forces for $f_r = 0{\cdot}80$ and $A/D = 0{\cdot}40$.

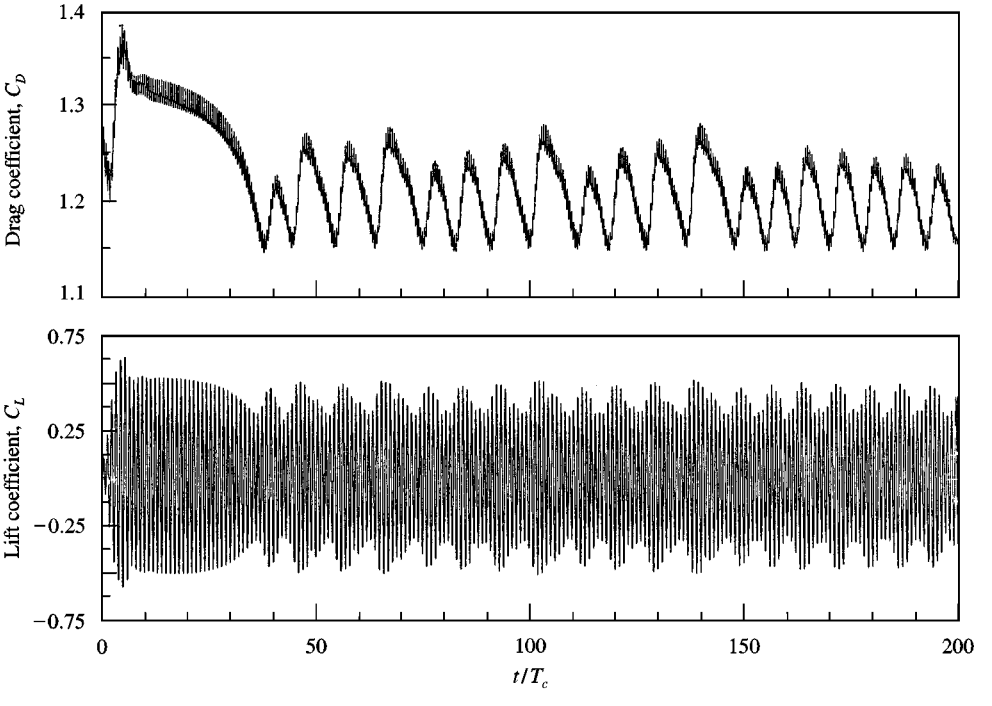

Figure 12. Time history of the hydrodynamic forces for $f_r = 1{\cdot}05$ and $A/D = 0{\cdot}11$.

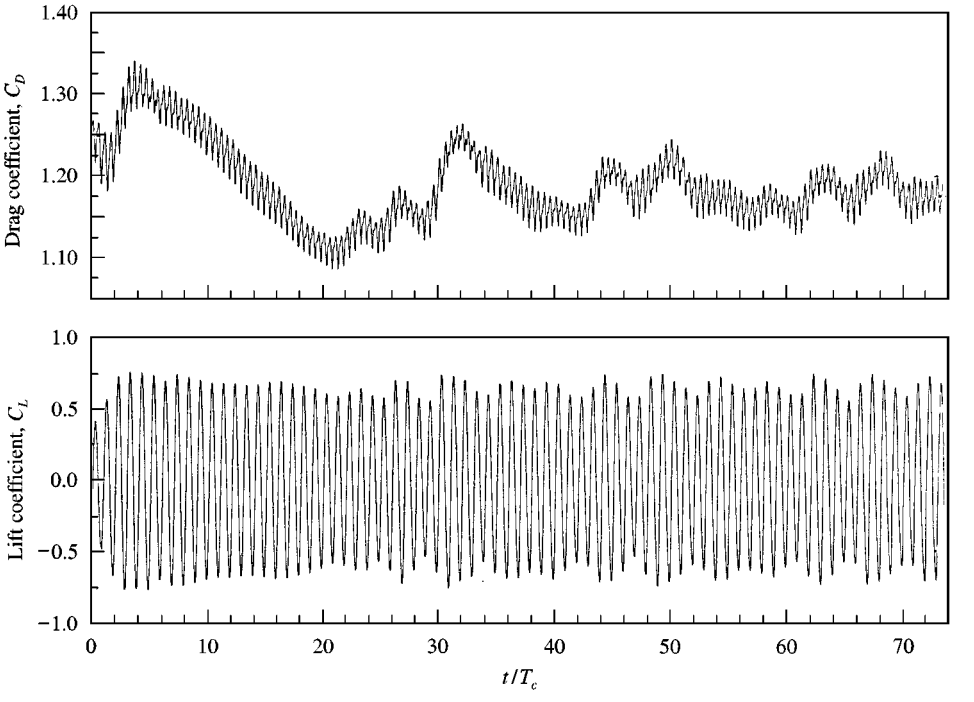

Figure 13. Time history of the hydrodynamic forces for $f_r = 1{\cdot}05$ and $A/D = 0{\cdot}20$.

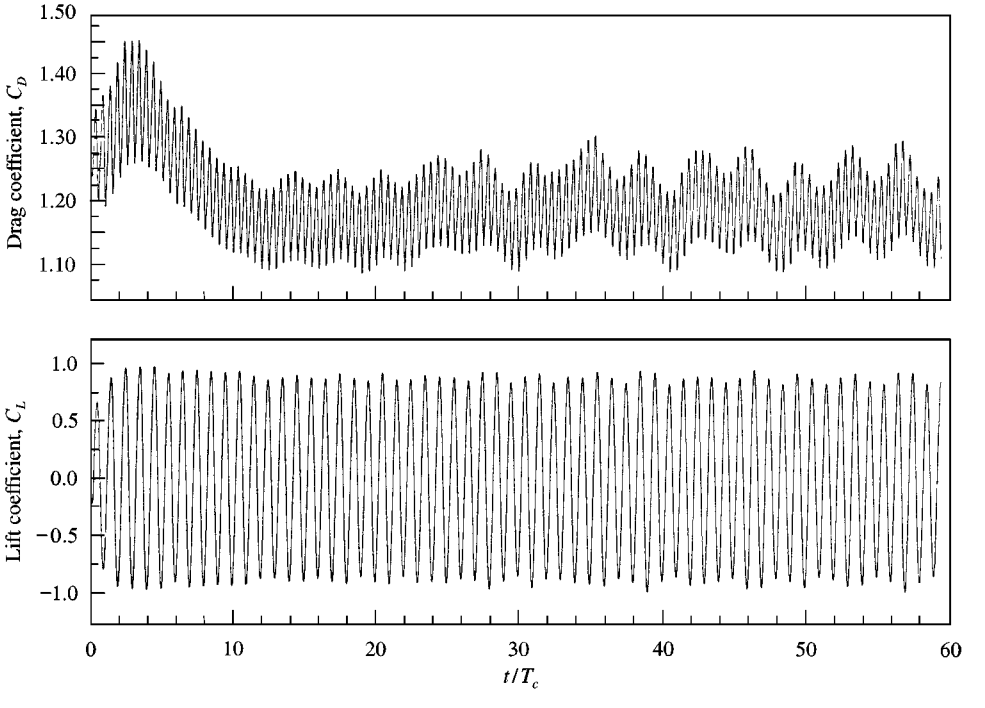

Figure 14. Time history of the hydrodynamic forces for $f_r = 1{\cdot}05$ and $A/D = 0{\cdot}30$.

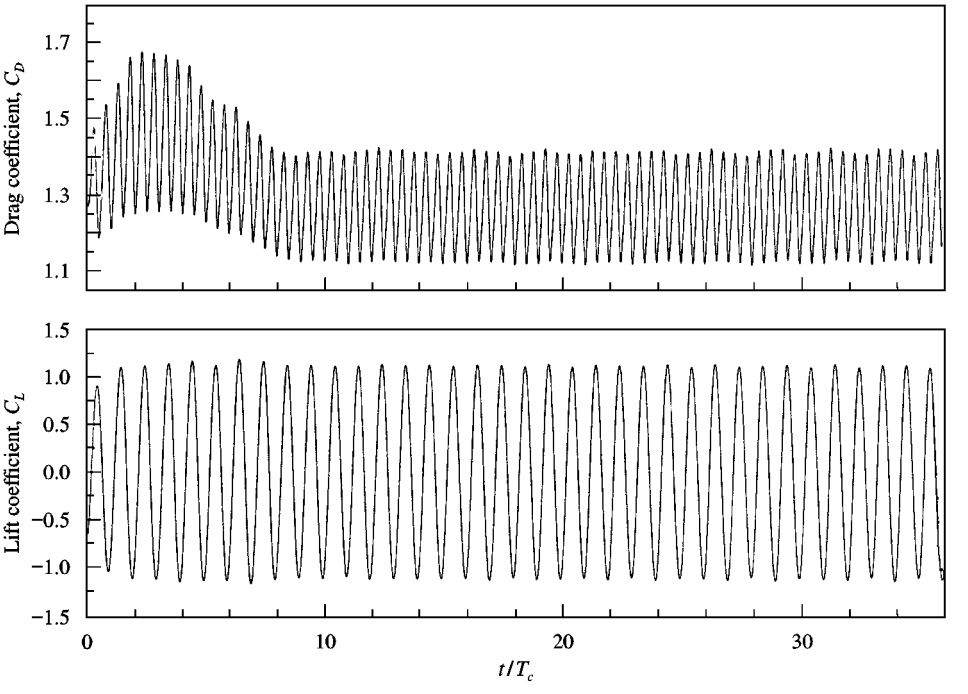

Figure 15. Time history of the hydrodynamic forces for $f_r = 1{\cdot}05$ and $A/D = 0{\cdot}40$.

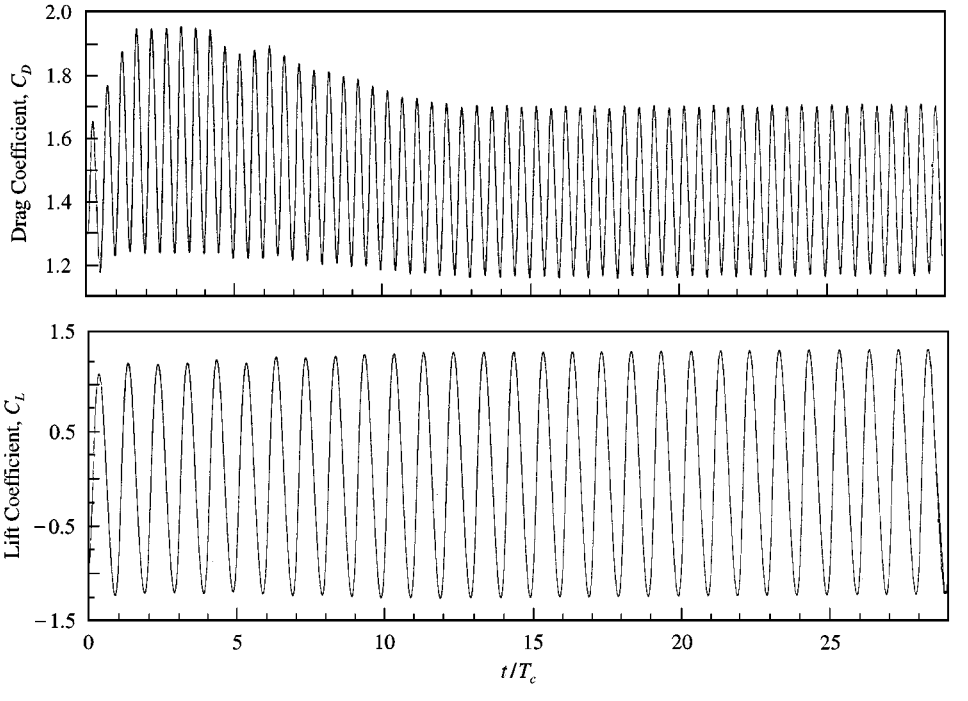

Figure 16. Time history of the hydrodynamic forces for $f_r = 1{\cdot}05$ and $A/D = 0{\cdot}50$.

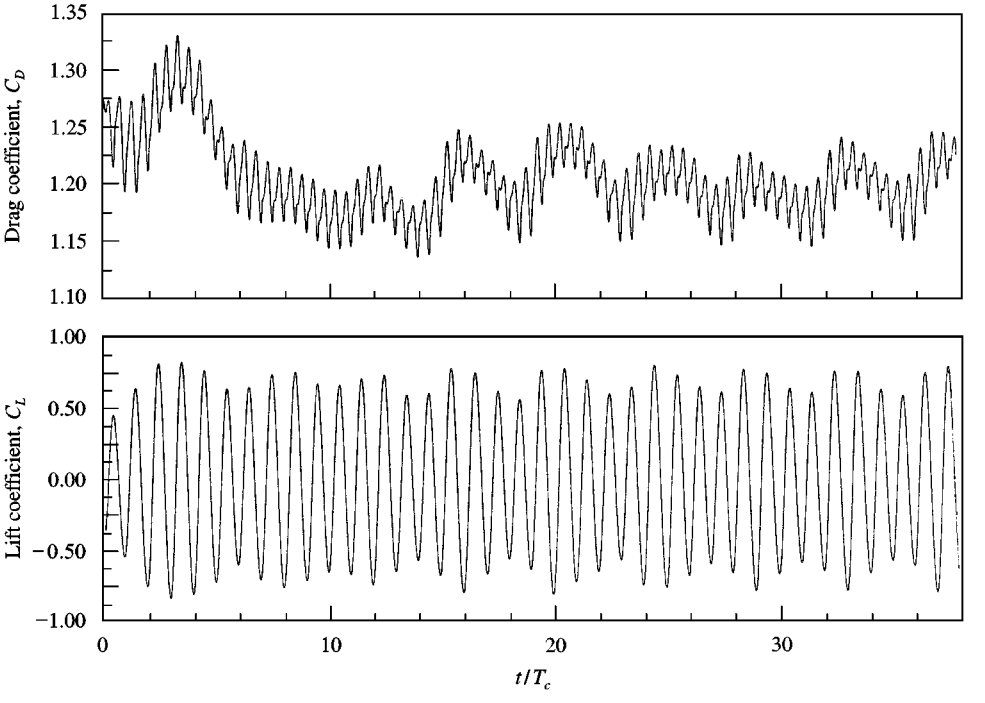

Figure 17. Time history of the hydrodynamic forces for $f_r = 1{\cdot}10$ and $A/D = 0{\cdot}20$.

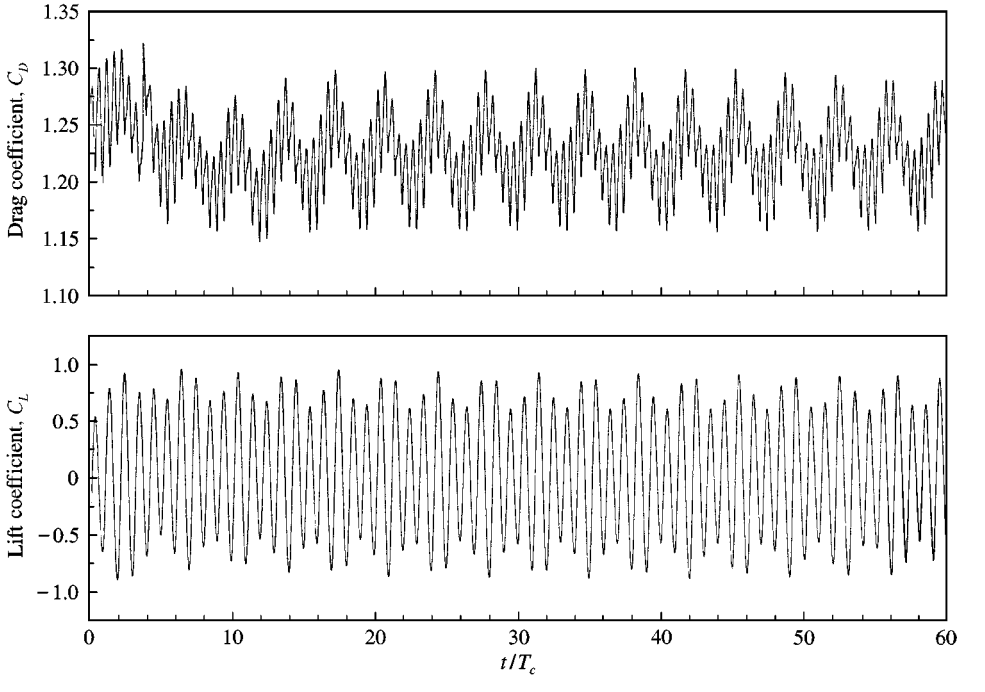

Figure 18. Time history of the hydrodynamic forces for $f_r = 1{\cdot}20$ and $A/D = 0{\cdot}20$.

sinusoidal. A power spectrum reveals the existence of a component at the natural shedding frequency, apart from the dominant peak at the cylinder oscillation frequency.

When f_r exceeds 1 the hydrodynamic forces are not periodic at subsequent cycles, except from the cases in which $A/D = 0{\cdot}50$. Figures 12–16 indicate that, when f_r equals 1·05, the hydrodynamic forces undergo a transient at the early stages from the inception of the cylinder motion, and afterwards the quasiperiodic or periodic (at $A/D = 0{\cdot}50$) state occurs. Examination of the same figures reveals that the number of periods required for the completion of the transient decreases as the oscillation amplitude is increased. For $A/D = 0{\cdot}11$ the transient is completed within 40 oscillation cycles, which are reduced to 12 as A/D is increased to 0·30. The force traces of Figures 13, 17 and 18 suggest that the increase of the oscillation frequency acts to reduce the number of cycles required for the completion of the transient.

The mean value of the dimensionless drag force exerted on the cylinder, the amplitude of the lift coefficient and the phase angle between the lift force and the cylinder displacement when periodicity or quasiperiodicity was reached, are depicted in Figures 19–21. The values of mean drag and lift amplitude in Figures 19 and 20 corresponding to a fixed cylinder ($A/D = 0$) were derived by Anagnostopoulos (1997) in the related study of vortex shedding past a fixed cylinder. For frequency ratios higher than 1 and in the range of oscillation amplitudes in which the traces are not periodic, average values were obtained from a sample containing many oscillation cycles, outside the initial transient. Figure 19 reveals that for $f_r \leq 1$ the increase of oscillation amplitude magnifies the mean drag when the oscillation frequency is maintained constant. Moreover, for constant amplitude of the cylinder oscillation, the drag force exerted on the cylinder decreases as the oscillation frequency is reduced

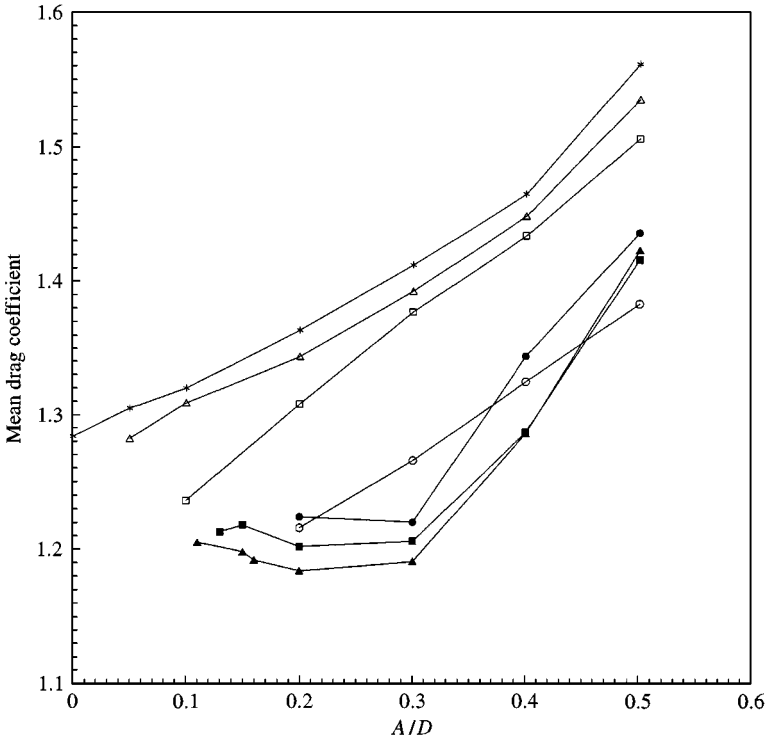

Figure 19. Mean value of the dimensionless drag force exerted on the cylinder inside the lock-in region: –○–, $f_c/f_s = 0{\cdot}80$; –□–, $f_c/f_s = 0{\cdot}90$; –△–, $f_c/f_s = 0{\cdot}95$; –*–, $f_c/f_s = 1{\cdot}00$; –▲–, $f_c/f_s = 1{\cdot}05$; –■–, $f_c/f_s = 1{\cdot}10$; –●–, $f_c/f_s = 1{\cdot}20$.

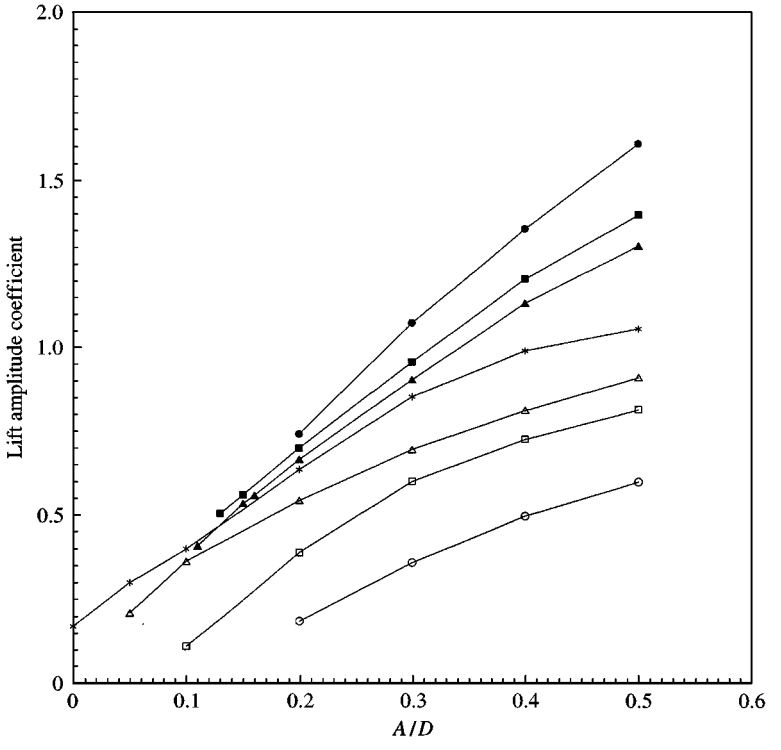

Figure 20. Amplitude of the lift coefficient within the lock-in region: –○–, $f_c/f_s = 0{\cdot}80$; –□–, $f_c/f_s = 0{\cdot}90$; –△–, $f_c/f_s = 0{\cdot}95$; –∗–, $f_c/f_s = 1{\cdot}00$; –▲–, $f_c/f_s = 1{\cdot}05$; –■–, $f_c/f_s = 1{\cdot}10$; –●–, $f_c/f_s = 1{\cdot}20$.

below the natural shedding frequency. The increase of the cylinder oscillation frequency above the natural shedding frequency causes reduction of the mean drag. For f_r higher than 1, the drag increases with increasing oscillation frequency when the amplitude is maintained constant. For constant oscillation frequency the drag experiences small fluctuations as the oscillation amplitude is increased from the lower limit of the lock-in boundary to 30% of the cylinder diameter. Then the drag increases substantially with the oscillation amplitude.

Figure 20 suggests that, when the oscillation frequency remains constant, the amplitude of the lift force exerted on the cylinder increases with the oscillation amplitude. On the other hand, when the oscillation amplitude remains the same, the lift amplitude increases continually as the frequency ratio is increased gradually from 0·80 to 1·20. It is interesting to note, that the amplitude of C_L at $f_r = 1{\cdot}20$ and $A/D = 0{\cdot}50$, is 10 times higher than the stationary cylinder value.

In the range of frequency ratios between 0·90 and 1, the phase angle, φ, between the lift force and the cylinder displacement decreases with increasing oscillation amplitude when the oscillation frequency is maintained constant. It is interesting to note the almost constant value of the phase angle for $f_r = 0{\cdot}80$ throughout the amplitudes examined in the lock-in region, and the abrupt decrease of φ in the low-amplitude regime when f_r equals 0·90 or 0·95. For $f_r > 1$ the effect of the frequency and amplitude of the cylinder oscillation on the phase angle is small, although a decrease is observed when f_r increases at constant amplitude. When the frequency ratio exceeds 1, the phase angle ranges between 26 and 36° throughout the lock-in region, much lower than in the cases when $f_r \leq 1$. The variation of the phase angle as the frequency and amplitude of oscillation are altered, is associated with the timing of vortex shedding past the moving cylinder.

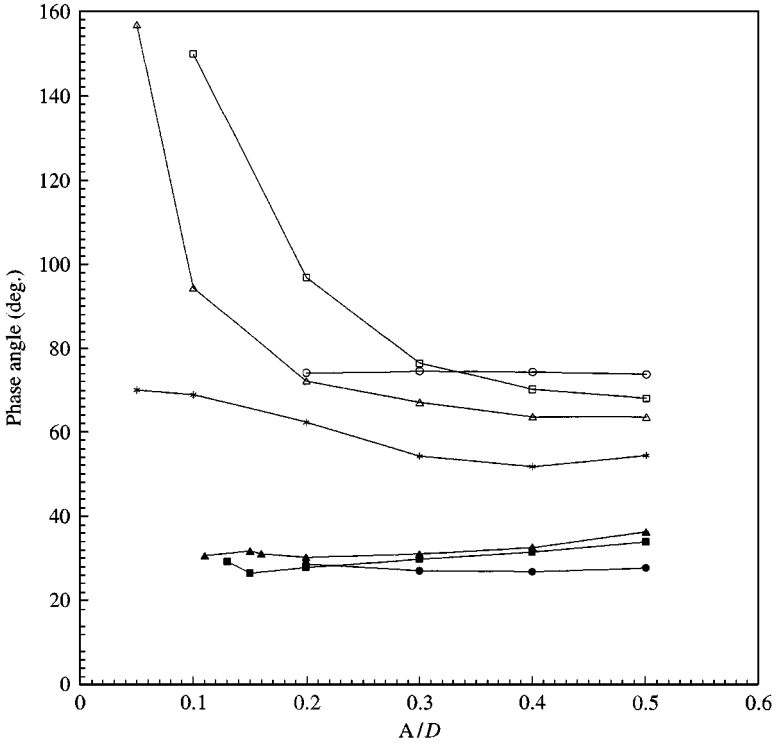

Figure 21. Phase angle between the lift force and the cylinder displacement: –○–, $f_c/f_s = 0{\cdot}80$; –□–, $f_c/f_s = 0{\cdot}90$; –△–, $f_c/f_s = 0{\cdot}95$; –∗–, $f_c/f_s = 1{\cdot}00$; –▲–, $f_c/f_s = 1{\cdot}05$; –■–, $f_c/f_s = 1{\cdot}10$; –●–, $f_c/f_s = 1{\cdot}20$.

The comparison of the present results to the experimental values of the drag force by Sarpkaya (1978) at Reynolds numbers in the range between 5000 and 25 000 and to the values of the drag, lift and phase angle measured by Gopalkrishnan (1993) at Re around 10 000 is interesting. The variations of the nondimensional mean drag and lift amplitude when the oscillation amplitude and frequency are altered follow the same trend, but the effect of the oscillation on the magnification of the mean drag is greater than that detected in the present study, especially in Sarpkaya's results. The phase angle in Gopalkrishnan's experiments decreases abruptly as the oscillation frequency is increased near resonance, throughout the amplitudes up to $A/D = 0{\cdot}50$. In the present study, this is the case only for $A/D = 0{\cdot}10$, whereas the phase angle experiences a milder decrease at higher oscillation amplitudes.

3.3. The Wake Geometry

To investigate the effect of the transverse cylinder motion of the vortex street wake the equi-vorticity lines were favoured, because their illustration is advantageous for the determination of the centres of the vortices. The equivorticity lines for various amplitudes and frequencies of oscillation when the flow has settled (corresponding to the periodic or quasiperiodic regime of the hydrodynamic forces) are presented in Figures 22–25. Throughout the study, the vorticity has been nondimensionalized from the formula $\zeta^* = \zeta D/2U$. For reasons of consistency the time instant depicted in all cases corresponds to the point of zero deflection, as the cylinder moves upwards. Figure 22, which illustrates the wake

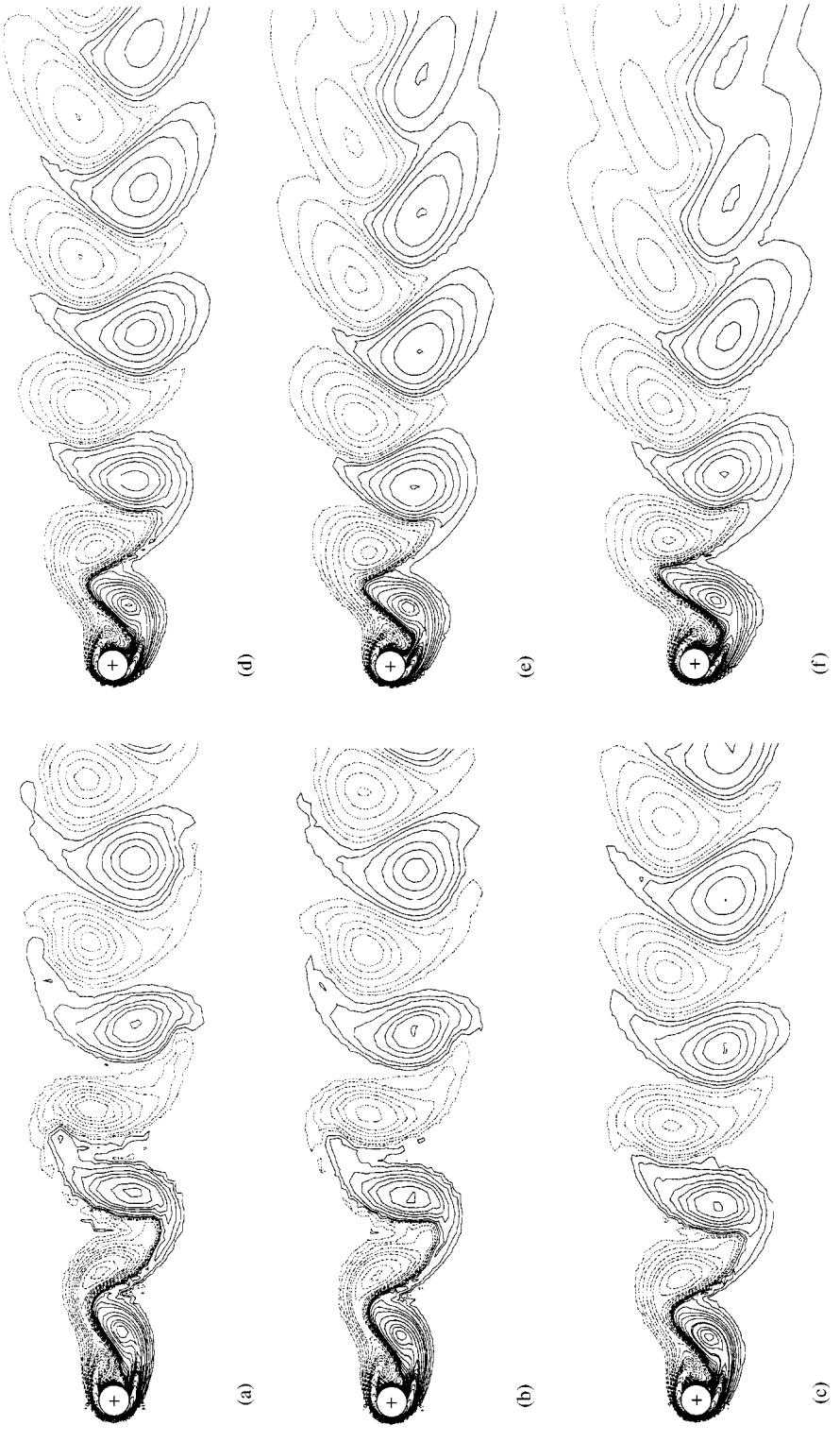

Figure 22. Equivorticity lines for $f_r = 1$ and A/D ranging between 0·05 and 0·50. The contours, starting from the outer vortex boundaries, correspond to the following values of dimensionless vorticity: 0·02, 0·05, 0·10, 0·20, 0·30, 0·40, 0·60. The full lines represent positive and the dashed negative vorticity. In all cases the cylinder passes from the undeflected position moving upwards: (a) $A/D = 0{\cdot}05$; (b) $A/D = 0{\cdot}10$; (c) $A/D = 0{\cdot}02$; (d) $A/D = 0{\cdot}30$; (e) $A/D = 0{\cdot}40$; (f) $A/D = 0{\cdot}50$.

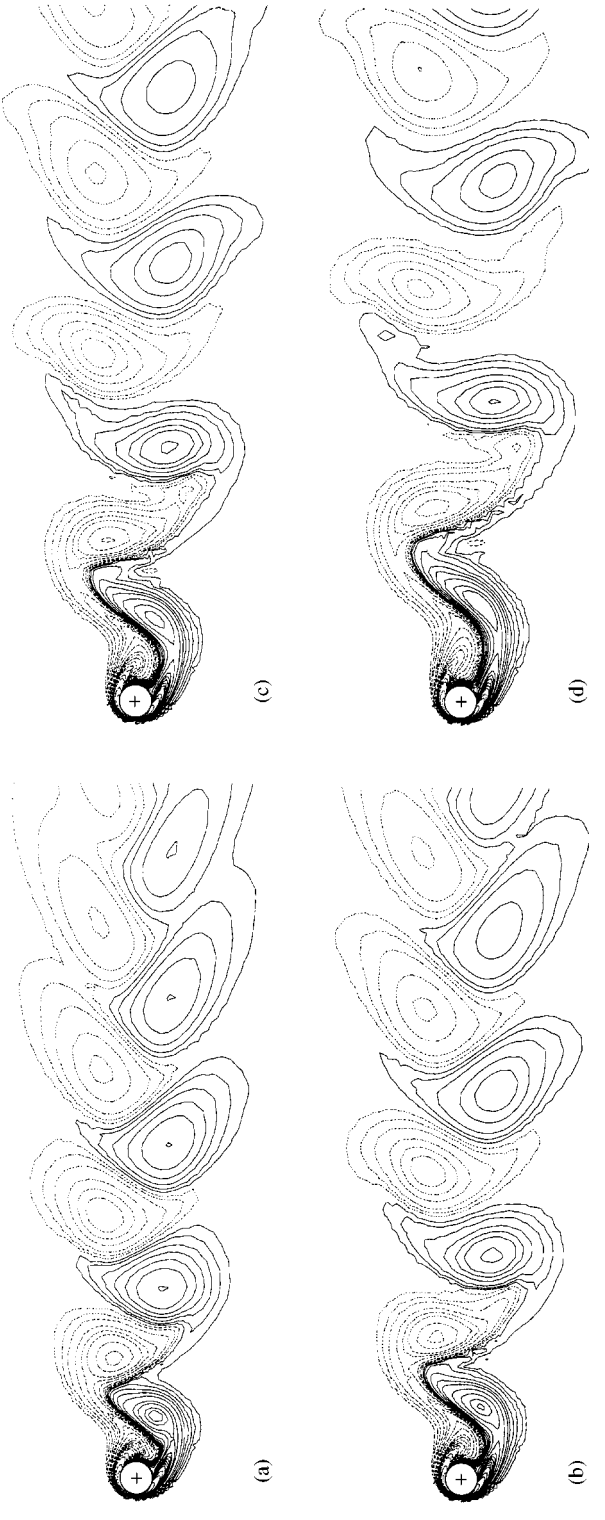

Figure 23. Equivorticity lines for $A/D = 0{\cdot}40$ and f_r ranging between 0·80 and 1. In all cases the cylinder passes from the undeflected position moving upwards: (a) $f_r = 1{\cdot}00$; (b) $f_r = 0{\cdot}95$; (c) $f_r = 0{\cdot}90$; (d) $f_r = 0{\cdot}80$.

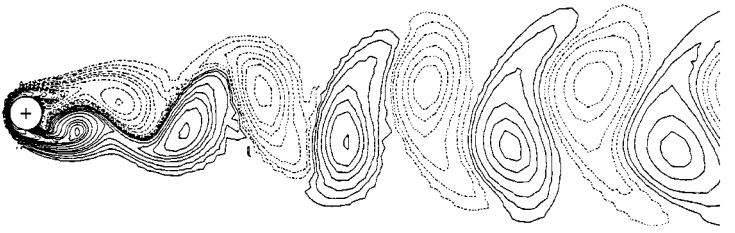

Figure 24. Vorticity contours for $f_r = 1{\cdot}05$ and $A/D = 0{\cdot}15$.

geometry for $f_r = 1$ and A/D extending up to 0·50, reveals that the longitudinal spacing, when stabilized, varies inversely with the oscillation amplitude for A/D in the range between 0·05 and 0·40. A further increase of A/D to 0·50 leaves the longitudinal spacing unaltered. The reduction of the longitudinal spacing at high amplitudes has as effect the coalescence of equal-sign vortices close to the downstream boundary, as depicted in Figure 22(e, f). On the other hand, the increase of the oscillation amplitude, acts to increase the spacing of vortices in the transverse direction. For the investigation of the effect of the oscillation frequency on the wake geometry, the equivorticity lines for constant A/D equal to 0·40 are depicted in Figure 23, when the frequency ratio varies between 0·80 and 1. These figures suggest that when A/D is maintained constant, both the longitudinal and the lateral spacing increase as the oscillation frequency of the cylinder decreases, the increase of the longitudinal spacing being more spectacular. The vorticity contours for $f_r = 1{\cdot}05$ and $A/D = 0{\cdot}15$ are depicted in Figure 24. This was an exceptional case in the range $f_r > 1$, since periodicity was maintained over several oscillation cycles at low amplitude. Comparison with frames 22(b) and 22(c) which illustrate the vorticity contours at $f_r = 1$ and A/D equal to 0·10 and 0·20, reveals that the timing of vortex shedding in these two frequency ratios is different, since the vortex being shed below the cylinder in Figure 24 is less developed than the corresponding vortices of frames 22(b) and 22(c). Moreover, the vortices close to the cylinder of Figure 24 appear rounder and less inclined to the horizontal than their counterparts in Figure 22(a, b).

Figure 25 indicates that for $f_r = 1{\cdot}10$, the vortex pattern is quite different from that observed when $f_r \leq 1$, throughout the amplitudes examined in the lock-in region. The vortex pattern is aperiodic and irregular, except from the case $A/D = 0{\cdot}50$ displayed in Figure 25(d). Nevertheless, even in Figure 25(d), the vortex spacing does not remain absolutely constant, especially in the streamwise direction. The situation remains the same, when f_r becomes equal to 1·05 and 1·20. An exception is the case $f_r = 1{\cdot}05$ and $A/D = 0{\cdot}15$ where a regular vortex street wake is maintained over a number of periods, as already stated.

It was mentioned previously that the aperiodic character of the hydrodynamic forces when f_r exceeds 1, hints to the nonperiodicity of the flow pattern. In an attempt to confirm this argument, the equivorticity lines for $f_r = 1{\cdot}05$ and $A/D = 0{\cdot}40$ at six time instants separated successively by an interval of one oscillation period are shown in Figure 26. In all frames, the cylinder deflection is very close to zero, as the cylinder moves upwards. Figure 26 shows clearly that the flow pattern is not periodic at consecutive cycles but periodicity is established every five oscillation cycles, a result which is compatible to the force traces of Figure 27. An interesting observation is the merging process occurring as the vortices are convected downstream, moving with different velocities. For example, the vortices U_3 and U_4 shed consecutively from the upper part of the cylinder coalesce to form one vortex, and the same happens for the vortices L_2 and L_3 shed from the lower part. The merging of adjacent vortices provides an explanation for the change of vortex spacing with increasing downstream distance from the cylinder.

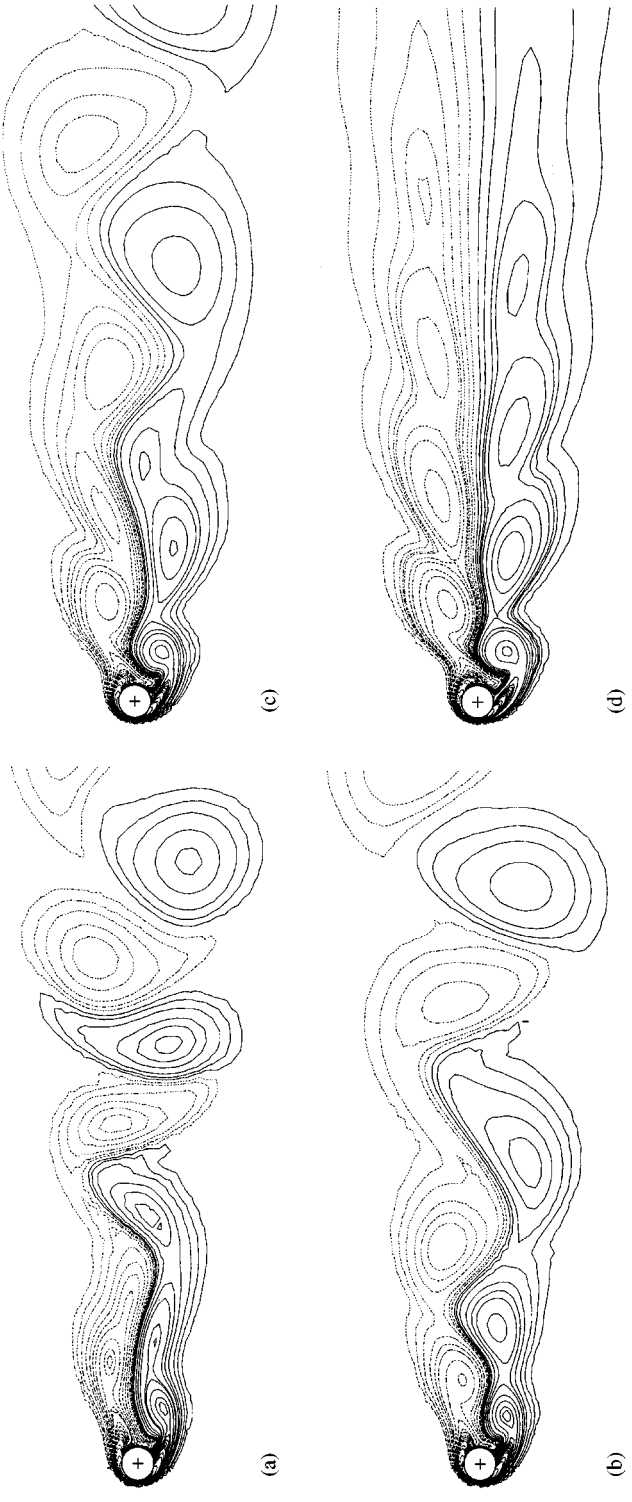

Figure 25. Equivorticity lines for $f_r = 1{\cdot}10$ and A/D ranging between 0·20 and 0·50: (a) $A/D = 0{\cdot}20$; (b) $A/D = 0{\cdot}30$; (c) $A/D = 0{\cdot}40$; (d) $A/D = 0{\cdot}50$.

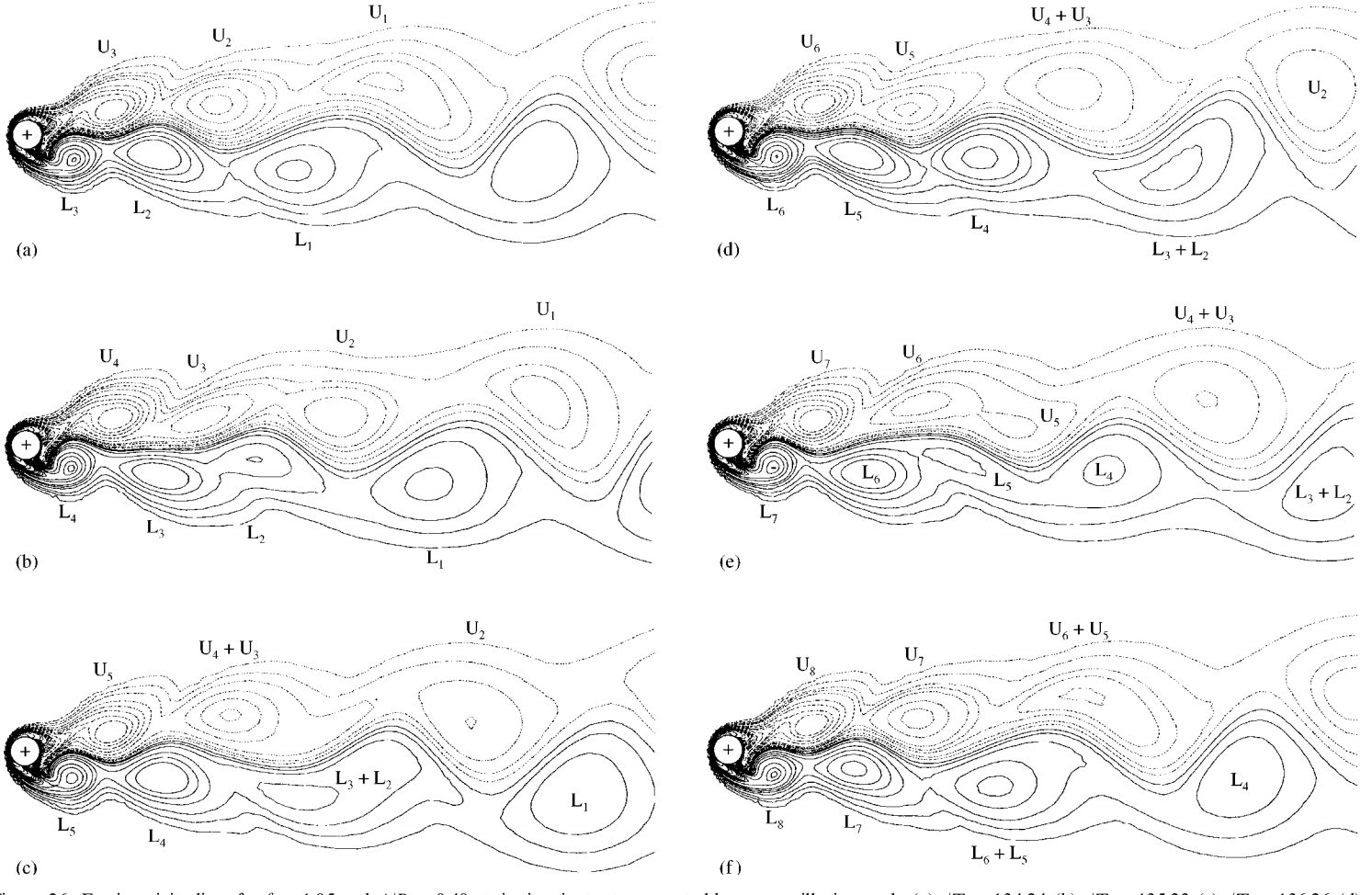

Figure 26. Equivorticity lines for $f_r = 1{\cdot}05$ and $A/D = 0{\cdot}40$ at six time instants separated by one oscillation cycle: (a) $t/T_c = 134{\cdot}24$; (b) $t/T_c = 135{\cdot}23$; (c) $t/T_c = 136{\cdot}26$; (d) $t/T_c = 137{\cdot}25$; (e) $t/T_c = 138{\cdot}24$; (f) $t/T_c = 139{\cdot}23$.

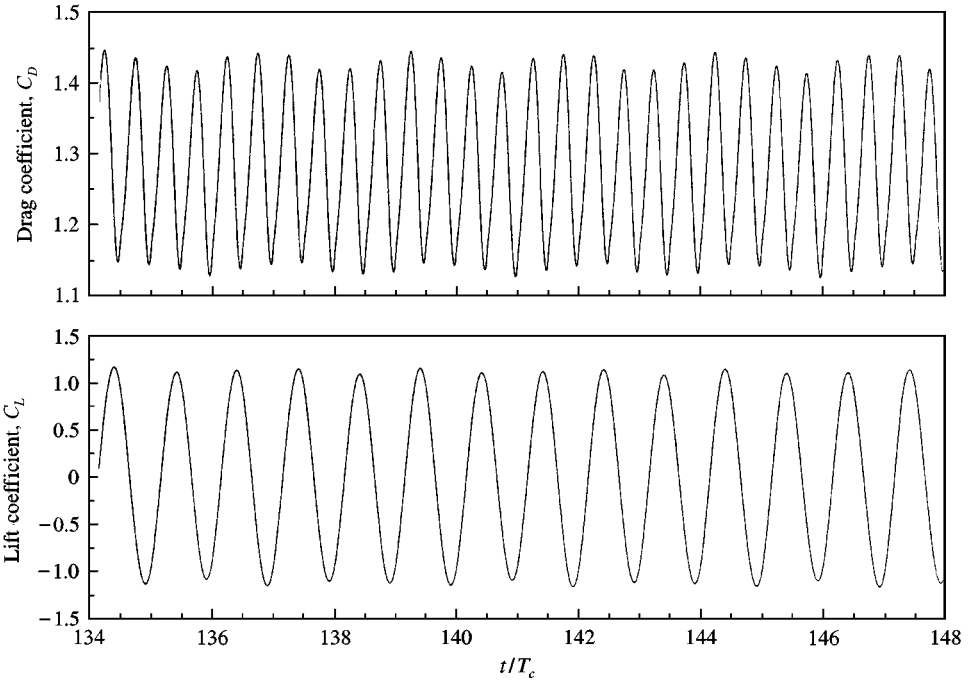

Figure 27. Traces of the hydrodynamic forces for $f_r = 1{\cdot}05$ and $A/D = 0{\cdot}40$, including the time instants at which the vorticity contours of Figure 26 are presented.

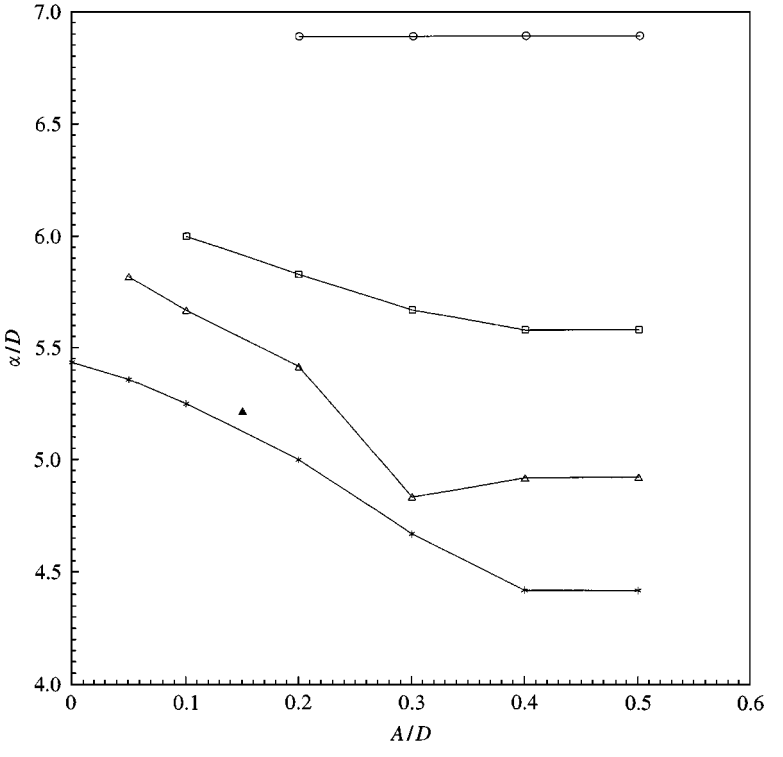

Figure 28. Spacing of vortices in the streamwise direction inside the lock-in region: –○–, $f_c/f_s = 0{\cdot}80$; –□–, $f_c/f_s = 0{\cdot}90$; –△–, $f_c/f_s = 0{\cdot}95$; –∗–, $f_c/f_s = 1{\cdot}00$; –▲–, $f_c/f_s = 1{\cdot}05$.

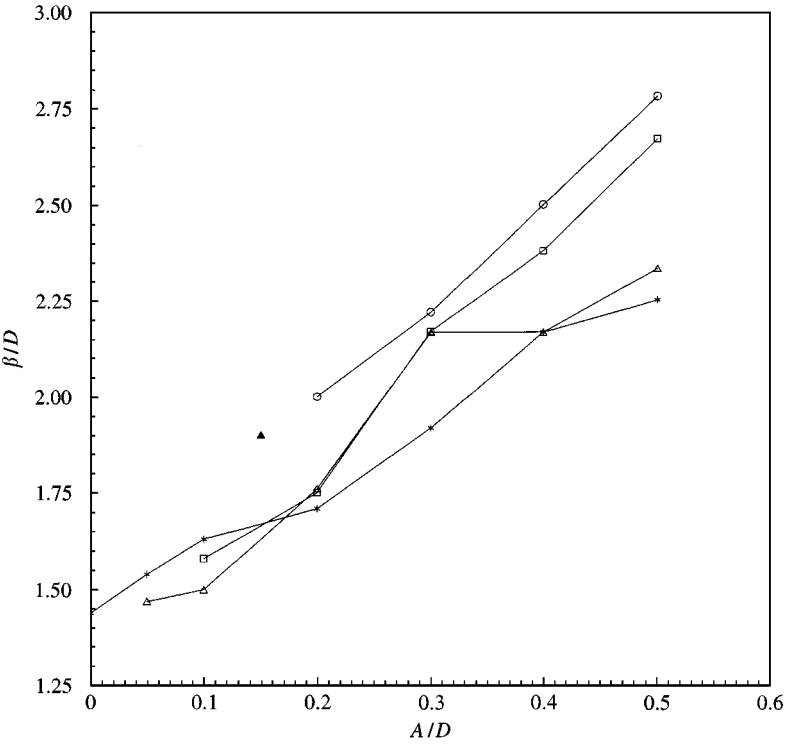

Figure 29. Spacing of vortices in the transverse direction inside the lock-in region: –○–, $f_c/f_s = 0{\cdot}80$; –□–, $f_c/f_s = 0{\cdot}90$; –△–, $f_c/f_s = 0{\cdot}95$; –∗–, $f_c/f_s = 1{\cdot}00$; –▲–, $f_c/f_s = 1{\cdot}05$.

The longitudinal spacing of vortices, denoted as α, for all oscillation frequencies and amplitudes examined for $f_r \leq 1$, is presented in Figure 28. For f_r equal to 0·90, 0·95 and 1 the longitudinal spacing decreases as the oscillation amplitude is increased to 0·40D. A further increase of A/D to 0·50 leaves the longitudinal spacing unaltered. It is interesting to note that for f_r equal to 0·80, the longitudinal spacing is independent of the oscillation amplitude. Figure 28 also reveals that when A/D is maintained constant, the longitudinal spacing increases as the oscillation frequency of the cylinder is decreased below the natural shedding frequency.

The lateral spacing of vortices, β, is summarized for $f_r \leq 1$ in Figure 29. When the oscillation frequency is maintained constant, the increase of the oscillation amplitude acts to magnify the vortex spacing in the lateral direction. On the the other hand, for constant oscillation amplitude, the lateral spacing of the vortices varies inversely with the frequency of the cylinder oscillation. This is not valid in the range of amplitudes $A/D < 0{\cdot}20$, in which the lateral spacing becomes maximum at $f_r = 1$. From Figures 28 and 29 it is interesting to note that the longitudinal and lateral spacings for the case when $f_r = 0{\cdot}95$ and $A/D = 0{\cdot}30$ fall outside the general trend. The computation was repeated for this case preclude a possible error in the computing process. A plausible explanation for the anomaly could be given.

The spacing ratio, β/α, is illustrated in Figure 30. When the oscillation frequency remains constant the increase of the amplitude causes magnification of the spacing ratio, while at constant oscillation amplitude, the spacing ratio decreases with decreasing oscillation frequency. A striking exception is the case when $f_r = 0{\cdot}95$ and $A/D = 0{\cdot}30$, as quoted previously.

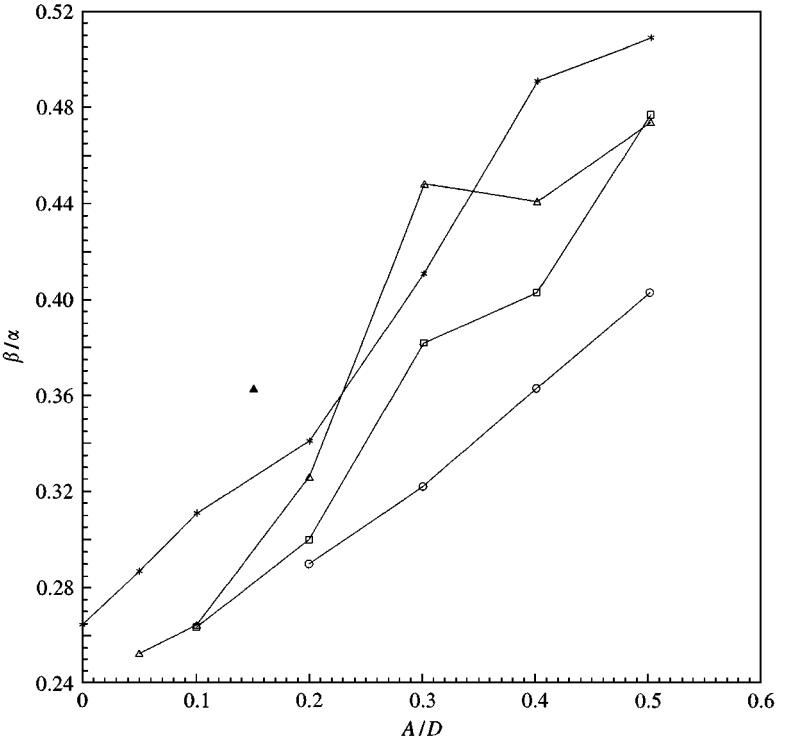

Figure 30. Vortex-spacing ratio within lock-in region: –○–, $f_c/f_s = 0{\cdot}80$; –□–, $f_c/f_s = 0{\cdot}90$; –△–, $f_c/f_s = 0{\cdot}95$; –∗–, $f_c/f_s = 1{\cdot}00$; –▲–, $f_c/f_s = 1{\cdot}05$.

4. CONCLUSIONS

The finite element technique was used for the investigation of laminar flow past a circular cylinder forced to oscillate transversely to the incident stream. When the frequency of the oscillating cylinder is equal or lower than the natural vortex-shedding frequency a periodic wake is formed behind the cylinder, whereas, when the oscillation frequency exceeds that of the natural shedding of vortices a quasiperiodic wake occurs, in which periodicity is established after a number of oscillation cycles. An exception is the case $A/D = 0{\cdot}50$, in which cycle-to-cycle periodicity was detected.

Due to the aperiodic character of the wake at $f_r > 1$, the velocity traces were favoured for the determination of the boundary of the lock-in zone, rather than the time histories of the hydrodynamic forces. The boundary of the lock-in region when $f_r < 1$ agrees considerably well with experimental evidence, while for $f_r > 1$ discrepancy with the experiment in some cases is observed.

The time histories of the hydrodynamic forces until periodicity or quasiperiodicity was established, were calculated for the various cases of the cylinder excitation. The flow settled after many oscillation cycles, especially for $f_r > 1$; thus extensive computer resources were required for the solution. The hydrodynamic forces and the phase angle between the lift force and the cylinder displacement within the lock-in region are presented in cumulative diagrams. These diagrams lead to the conclusion that when the oscillation frequency remains constant, the mean drag and the lift amplitude increase with the oscillation amplitude, whereas for constant oscillation amplitude the increased value of oscillation frequency magnify the amplitude of the lift force. The phase angle between the fluctuating

lift force and the cylinder displacement decreases as the oscillation amplitude is increased at constant frequency in the range between 1 and 0·90, whereas, for frequency ratio equal to 0·80 the phase angle remains almost constant. When f_r exceeds 1 the change of the oscillation parameters have little effect on the phase angle, which remains substantially lower compared to the cases when $f_r \geq 1$.

In spite of the periodic character of the flow observed for $A/D = 0{\cdot}50$ when f_r exceeds 1, the vortex spacing, especially the longitudinal one, is altered with downstream distance from the cylinder. Thus, results concerning the vortex spacing were presented only for $f_r \leq 1$, an exception being the case $f_r = 1{\cdot}05$ and $A/D = 0{\cdot}15$. For constant oscillation frequency, the increase of the oscillation amplitude leads to reduced longitudinal and increased lateral spacing of the vortices, while the spacing in both directions increases as the oscillation frequency is reduced at constant amplitude. An exception in the case when f_r equals to 0·80, in which the longitudinal spacing remains constant throughout the range of amplitudes examined inside lock-in.

References

Akbari, M. H. & Price, S. J. 1997 Simulation of the incompressible viscous cross-flow around an oscillating circular cylinder via the random vortex method. In *Proceedings of the Fourth International Symposium on Fluid–Structure Interactions, Aeroelasticity, Flow-Induced Vibration and Noise* (eds M. P. Paidoussis *et al.*), Vol. 1, pp. 21–32. New York: ASME.

Anagnostopoulos, P. 1989 Numerical solution for laminar two-dimensional flow about a fixed and transversely oscillating cylinder in a uniform stream. *Journal of Computational Physics* **85,** 434–456.

Anagnostopoulos, P. 1994 Numerical investigation of response and wake characteristics of a vortex-excited cylinder in a uniform stream. *Journal of Fluids and Structures* **8,** 367–390.

Anagnostopoulos, P. 1997 Computer-aided flow visualization and vorticity balance in the laminar wake of a circular cylinder. *Journal of Fluids and Structures* **11,** 33–72.

Anagnostopoulos, P. & Bearman, P. W. 1992 Response characteristics of a vortex-excited cylinder at low Reynolds numbers. *Journal of Fluids and Structures* **6,** 39–50.

Bearman, P. W. & Currie, I. G. 1979 Pressure fluctuation measurements on an oscillating circular cylinder. *Journal of Fluid Mechanics* **91,** 661–677.

Blevins, R. D. 1994 *Flow-Induced Vibration*, 2nd edition. New York: Krieger Publishing Company.

Bishop, R. E. D. & Hassan, A. Y. 1964 The lift and drag forces on a circular cylinder oscillating in a flowing fluid. *Proceedings of the Royal Society of London, Series A* **277,** 51–75.

Brika, D. & Laneville, A. 1993 Vortex-induced vibrations of a long flexible circular cylinder. *Journal of Fluid Mechanics* **250,** 481–508.

Cheng, M. & Moretti, P. M. 1991 Lock-in phenomena on a single cylinder with forced transverse oscillation. In *Flow-induced Vibration and Wear*, ASME PVP-Vol. 206, pp 129–133.

Chilukuri, R. 1987 Incompressible laminar flow past a transversely vibrating cylinder. *ASME Journal of Fluids Engineering* **109,** 166–171.

Copeland, G. S. & Cheng, B. H. 1995 Hysteretic vortex shedding from an oscillating cylinder. In *Proceedings of the Sixth International Conference on Flow-Induced Vibration* (ed. P. W. Bearman), pp. 221–230, London, U.K. Rotterdam: A.A. Balkema.

Feng, C. C. 1968 The measurement of vortex-induced effects in flow past stationary and oscillating circulator and D-section cylinder. M.Sc. thesis, University of British Columbia, Vancouver, B.C., Canada.

Gopalkrishnan, R. 1993 Vortex-induced forces on oscillating bluff cylinders. Ph.D. thesis, MIT, Cambridge, MA, U.S.A.

Griffin, O. M. 1971 The unsteady wake of an oscillating cylinder at low Reynolds number. *Journal of Applied Mechanics* **38,** 729–738.

Griffin, O. M. & Ramberg, S. E. 1974 The vortex-street wakes of vibrating cylinders. *Journal of Fluid Mechanics* **66,** 553–576.

Griffin, O. M. & Hall, M. S. 1995 Vortex shedding lock-on in a circular cylinder wake. In *Proceedings of the Sixth International Conference on Flow-Induced Vibration* (ed. P.W. Bearman), pp. 3–14, London, U.K. Rotterdam: A.A. Balkema.

Gu, W., Chyu, C. & Rockwell, D. 1994 Timing of vortex formation from an oscillating cylinder. *Physics of Fluids* **6,** 3677–3682.

Honji, H. & Taneda, S. 1968 Vortex wakes of oscillating circular cylinders. *Reports of Research Institute for Applied Mechanics, Kyushu* **16,** 211–222.

Hurlbut, M., Spaulding, M. L. & White, F. M. 1982 Numerical solution for laminar two dimensional flow about a cylinder oscillating in a uniform stream. *ASME Journal of Fluids Engineering* **104,** 214–222.

Karniadakis, G. & Triantafyllou, G. 1989 Frequency selection and asymptotic states in laminar wakes. *Journal of Fluid Mechanics* **199,** 441–469.

Koopmann, G. H. 1967 The vortex wakes of vibrating cylinders at low Reynolds numbers. *Journal of Fluid Mechanics* **27,** 501–512.

Lecointe, Y. & Piquet, J. 1989 Flow structure in the wake of an oscillating cylinder. *ASME Journal of Fluids Engineering* **111,** 139–148.

Lu, X.-Y. & Dalton, C. 1996 Calculation of the timing of vortex formation from an oscillating cylinder. *Journal of Fluids and Structures* **10,** 527–541.

Meneghini, J. R. & Bearman, P. W. 1995 Numerical simulation of high amplitude oscillatory flow about a circular cylinder. *Journal of Fluids and Structures* **9,** 435–455.

Mittal, S. & Tezduyar, T. E. 1992 A finite element study of incompressible flows past oscillating cylinders and airfoils. *International Journal for Numerical Methods in Fluids* **15,** 1073–1118.

Nomura, T. 1993 Finite element analysis of vortex-induced vibrations of bluff cylinders. *Journal of Wind Engineering and Industrial Aerodynamics* **46–47,** 587–594.

Ongoren, A. & Rockwell, D. 1988 Flow structure from an oscillating cylinder. Part 1: Mechanisms of phase shift and recovery in the near wake. *Journal of Fluid Mechanics* **191,** 197–223.

Sarpkaya, T. 1978 Fluid forces on oscillating cylinders. *ASCE Journal of the Waterway, Port, Coastal and Ocean Division* **104,** 275–290.

Sarpkaya, T. & Shoaff, R. L. 1979 A discrete vortex analysis of flow about stationary and transversely oscillating circular cylinders. Technical Report No. NPS-69SL79011, Naval Postgraduate School, Monterey, Cal., USA.

Stansby, P. 1976 The locking-on of vortex shedding due to the cross-stream vibration of circular cylinders in uniform and shear flows. *Journal of Fluid Mechanics* **74,** 641–665.

Wei, R., Sekine, A. & Shimura, M. 1995 Numerical analysis of 2D vortex-induced oscillations of a circular cylinder. *International Journal for Numerical Methods in Fluids* **21,** 993–1005.

Williamson, C. H. K. & Roshko, A. 1988 Vortex formation in the wake of an oscillating cylinder. *Journal of Fluids and Structures* **2,** 355–381.

Zdravkovich, M. M. 1982 Modification of vortex shedding in the synchronization range. *ASME Journal of Fluids Engineering* **104,** 513–517.

Zhang, J. & Dalton, C. 1997 Interaction of a steady approach flow and a circular cylinder undergoing forced oscillation. *ASME Journal of Fluids Engineering* **119,** 808–813.